Journal of Building Engineering 105 (2025) 112570

Contents lists available at ScienceDirect

Journal of Building Engineering

journal homepage: www.elsevier.com/locate/jobe

Effect of graphene oxide on interfacial transition zone and strength enhancement of recycled aggregate concrete

Pasadi Devapura [a,*], Thusitha Ginigaddara [a], Danula Udumulla [a], Priyan Mendis [a], Michael Booy [b], Nilupa Herath [a]

[a] Department of Infrastructure Engineering, The University of Melbourne, Parkville, VIC, 3010, Australia
[b] Heidelberg Materials Pty Ltd., Brisbane, QLD, 4000, Australia

ARTICLE INFO

Author keywords:
Graphene oxide
Recycled concrete aggregates
Interfacial transition zone
Microstructure

ABSTRACT

This study reports the use of graphene oxide (GO) as an additive for performance enhancement of concrete containing a high volume of recycled aggregates. The current industry practice of incorporating recycled concrete aggregates (RCA) in concrete is limited to ~30 % replacement of natural coarse aggregates (NCA) in concrete and non-structural applications. The targeted approach of this research is to increase this replacement level to 50 % using GO as a performance enhancer and to investigate the effects of GO on the interfacial transition zones (ITZ). Five concrete mixes were made including 100 % NCA (as a benchmark), 50 % RCA (as a control) and GO admixed recycled aggregate concrete (RAC). The dosage of GO in the mixes were 0.015 %, 0.035 % and 0.065 % by weight of cement. Fresh and hardened properties such as workability, compressive strength, splitting tensile and elastic moduli were evaluated in this study. In addition, the characteristics of the ITZs were examined by scanning electron microscope (SEM) and energy dispersive spectroscopy (EDS). The results conclude that the addition of GO at 0.015 %, 0.035 % and 0.065 % enhances the 28-day compressive strength by 4 %, 35 % and 34 % respectively. SEM/EDS evaluations revealed that the widths of three ITZs associated with RCA have improved by the addition of 0.035 % GO. The incorporation of GO has densified the microstructure and reduced the ITZ widths by approximately 40–50 % which agrees well with the mechanical properties. The outcomes of this research provide instrumental scientific evidence that can encourage the industry to replace higher factions of NCA with RCA.

1. Introduction

Greenhouse gas (GHG) emissions and global warming have become a critical global concern. Since 1990, CO_2 emissions from energy combustion and industrial processes have surged from 2.0 Gt to a highest ever recorded of 36.8 Gt in 2022 [1,2]. At this rate, the global mean temperature is expected to rise by ~5 °C as forecasted by the International Energy Agency (IEA) [3]. Population growth, urbanization, and industrialization contribute to this upward trend in GHG emissions with projections indicating further increases if emissions are not effectively controlled or mitigated. Supporting this, the Paris Climate Agreement encourages nations to mitigate emissions and achieve Net Zero status by the year 2050 [4]. In this context, nations are increasingly adopting sustainable development practices, emphasizing reduced natural resource consumption in the construction industry.

* Corresponding author.
E-mail address: pdevapura@student.unimelb.edu.au (P. Devapura).

https://doi.org/10.1016/j.jobe.2025.112570
Received 2 February 2025; Received in revised form 25 March 2025; Accepted 3 April 2025
Available online 4 April 2025

Concrete is not only the predominant construction material in the world but also the second most consumed material globally. However, as a composite, a large fraction of concrete consists of natural constituents such as coarse aggregates, sand, and limestone. Extraction of these natural resources for concrete production has led to their depletion and adversely affected the environment. In addition, concrete construction and demolition waste (CDW) has emerged as a pressing issue in terms of solid waste management and landfills. Since 2012, more than 3 billion tons of CDW has been generated globally, and continues to rise [5]. Moreover, within the context of industrial emissions, the cement industry is accountable for approximately 5–7 % of annual global GHG emissions. On average, it is reported that each ton of cement manufactured releases an equivalent amount of anthropogenic CO_2 to the atmosphere. Over the past few decades, the global demand for cement has increased reflecting to a corresponding rapid growth in CO_2 emissions associated with its manufacturing process. From a sustainable point of view, the efficient upcycling of CDW into recycled concrete aggregate (RCA) presents a promising solution for the construction industry to mitigate exploitation of natural coarse aggregates (NCA), CDW disposal in landfills, and climate change impact to achieve net-zero emissions.

CDW, which comprises of a heterogenous mix of concrete, mortar, bricks, mineral aggregates and other materials are industrially processed to manufacture RCA [6]. Research studies indicate that RCA can be incorporated in concrete mixtures as an effective replacement for NCA [7–9]. However, the quality of RCA significantly varies based on several factors such as the grade of the original concrete, demolition methods, contamination levels and the production process which affects the performance of Recycled aggregate concrete (RAC). It comprises of inherent drawbacks, including high water absorption, weak interfacial transition zones (ITZs), and inferior mechanical and durability properties. These issues are primarily attributed to adhered old mortar (OM) on RCA, which constitutes approximately 35 % or more of its volume, and the micro-cracks introduced during the crushing process [10,11]. Compared to NCA, RCA exhibits a significantly higher water absorption capacity (4.5–8 % vs. <1 %), leading to poor workability and lower mechanical properties in RAC [12,13]. The triple ITZs in RAC also plays a pivotal role in its mechanical and durability performance. As illustrated in Fig. 1, the triple ITZs consists of:

1. The **old ITZ**, located between old virgin aggregate (VA) and OM, characterized by high porosity and weak bonding.
2. The **new ITZ 1**, forming between the OM and the new mortar (NM).
3. The **new ITZ 2**, forming between VA and NM.

The high porosity and weak bonding within the ITZs of RAC significantly contribute to its inferior mechanical properties. Consequently, enhancing the quality of RCA is essential for improving the overall performance of RAC. Sae-Long et al. (2024) highlights the critical influence of ITZs on RAC's damage behaviour through numerical simulations based on composite damage theory [14]. To investigate the microstructural characteristics of ITZs, researchers have employed various advanced techniques, including scanning electron microscopy (SEM) with energy-dispersive spectroscopy (EDS) [15], mercury intrusion porosimetry (MIP) [16], computed tomography (CT) [17], Vickers hardness testing [18], and nanoindentation [19]. These methods provide insights into ITZ's porosity, microhardness, and thickness, which are crucial parameters affecting RAC durability and strength.

Simultaneously, various methods have been developed to remove OM and improve RCA quality. Mechanical grinding, thermal treatment, and chemical soaking are commonly employed methods for removing OM [20–22]. While effective in reducing water absorption and improving aggregate density, these methods have limitations such as secondary damages to RCA, high energy consumption, hazardous waste generation, and increased carbon emissions. For instance, mechanical grinding emits nearly twice the CO_2 compared to thermal methods [23,24] which hinders the large-scale adoption of such approaches [25].

Several research studies conclude that substitutions up to 20 % of NCA with RCA has no detrimental effect on the properties of RAC [26–28]. Countries such as Brazil, China, Germany, and United Kingdom [29–32] have initiated setting specifications for the use of RCA. However, these specifications typically limit its inclusion based on the type of application, desired concrete strength class and the

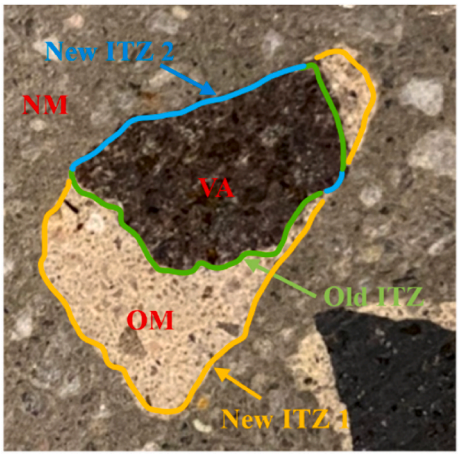

Fig. 1. Old and new ITZs in RA concrete.

properties of RCA. In Australia, present guidelines recommend partial replacement of ~30 % of NCA with RCA for concrete (typically up to 32 MPa) without compromising the mechanical properties [33,34]. Generally, the applications for RAC are limited to low-risk, non-structural applications such as road base, pavements, foundational materials, and pipe beddings, and low-grade concretes (below C40). Sae-Long et al. (2024) validated this through finite element simulations in a comprehensive study on RCA and para-wood ash concrete, concluding that despite the reduction in strength, it remains suitable for engineering applications requiring light loads and low to medium strength [14]. Moreover, the lack of international standards addressing the use of RCA impairs the industrial use in structural concrete.

Instead of removing OM, strengthening methods such as carbonation and pre-coating strategies are gaining traction. Carbonation involves reacting OM with CO_2 to form denser calcium carbonate, improving RCA strength and ITZ quality [35]. Pre-coating RCA with materials like sodium silicates, polymer emulsions, and nano-silica slurry can reduce water absorption, but some coatings such as hydrophobic polymers weaken the bond between aggregates and cement [36,37]. The use of bio-deposition and self-healing agents, though promising, requires further research to address durability challenges in severe exposure conditions [38]. However, both OM removal and strengthening methods often incur significant environmental and production costs. For example, CO_2 emissions from pretreatment processes and disposal of mortar waste highlight the need for more sustainable solutions. In industrial cases where no pre-treatment methods are employed to enhance the quality of RCA, additional cementitious materials or increased Ordinary Portland Cement (OPC) content are introduced to offset the mechanical limitations of untreated RCA. However, this practice significantly increases the embodied CO_2 content of RAC, compounding environmental concerns.

Considering these limitations, alternative approaches that balance mechanical performance with environmental sustainability are increasingly pursued for the development of low-emission concrete. One such innovation is the incorporation of very low dosages of Graphene Oxide (GO), a nanomaterial with transformative potential for cement-based composites. GO's two-dimensional (2D) structure, oxygenated functional groups, and excellent dispersibility in water enable significant improvements in concrete performance even at low dosages such as 0.02–0.1 % by weight of cement (bwoc) [39–41]. Leveraging these unique properties, GO not only enhances hydration reactions but reduces microstructural voids, resulting in compressive strength improvements of up to 39 % in concrete [42]. Beyond mechanical enhancements, GO's ability to optimize cement usage offers a dual advantage, improving concrete performance while significantly reducing its environmental footprint. Studies have shown that GO reduces the embodied CO_2 of concrete up to 30 %, making it an environmentally favourable alternative over traditional methods [43]. This dual impact positions GO as a viable solution for the challenges faced in sustainable concrete practices, setting the stage for further exploration of its capabilities.

However, integration of GO into cementitious systems still face challenges such as inadequate dispersibility [44,45] owing to high alkalinity and divalent calcium ions in cement which promote agglomerations [46], compromise performance enhancements [47] and produce inconsistent results [48]. Previous studies have reported that GO undergoes partial reduction and structural degradation in cementitious environments (pH $>$ 12.5), leading to a loss of oxygenated functional groups and diminished reinforcement efficiency [46,49,50]. Therefore, researchers have employed a combination of advanced mixing techniques and chemical surface modifications to enhance the dispersion efficiency, chemical retention, and stability of GO in highly alkaline environments. Common mixing methods include high-shear mixing, ultrasonication, and electromagnetic stirring [51,52], while chemical modification techniques include the use of surfactants such as polycarboxylate ethers (PCE), sodium dodecylbenzene sulfonates, lignosulfonates and anionic agents [53–55]. The advanced mixing methods disintegrate stacked GO sheets by weakening van der Waals forces, exposing more functional groups for improved interactions in aqueous environments [56] while chemical modifications introduce electrostatic repulsion and steric hindrance for improved dispersibility in cement matrix [57]. Amongst these, PCE-based superplasticizers and ultrasonication are widely recognized as useful techniques for minimizing GO agglomeration and improving dispersion in cementitious composites [58]. For an instance, Anwar et al. (2024) suggest post-processing techniques for synthesized GO powder such as heat assisted magnetic stirring for 2 h and sonication of GO in PCE-containing water [59]. Devi et al. (2020) also reports a similar process which involves 30 min of ultrasonication followed by magnetic stirring of GO with total water content and PCE of the concrete mix [60]. However, Silvestro et al. (2022) and Poinot et al. (2013) argue that advanced mixing methods adopted above (particularly ultrasonication) reduces the length of polymer lateral chains in PCE, compromising fresh and hardened properties of concrete [61,62]. Moreover, integration of such advanced mixing equipment, infrastructure modifications at batching plants, complex CO_2 and energy intensive processes hinder large-scale adoption of GO induced concrete production. Addressing these limitations, this study introduces a simplified approach where a significantly shorter ultrasonication time is included as a part of GO synthesis process and dispersion of GO in concrete is achieved through a simple manual mixing method.

In addition, studies in this domain often lack detailed information on the raw materials used for GO synthesis, parameters of chemical reactions, and characterizations [63–65]. Synthesis methods employed by commercial suppliers are typically proprietary and vary significantly between manufacturers. For an instance, Djenaoucine et al. (2024) reports improvements in hydration (by 7 %), flexural strength (by 31 %) and compressive strength (9 %) in cement mortar at 28 days but does not specify the GO dosage used due to confidentiality agreements with the supplier [63]. This limits the reproducibility of research findings [66] and complicates the interpretation of GO characteristics along with its interactions in cementitious materials. Additionally, a comparison between Ginigaddara et al. (2023) [67] and Krystek et al. (2019) [68] reports conflicting findings on 28-day compressive strength enhancement at a 0.05 % GO dosage, despite both studies maintaining the same w/c ratio of 0.5. The former study used GO sourced from Ceylon Graphene Technologies, reported a 12 % strength increase, whereas Krystek et al., using GO from Graphenea, observed an 11 % strength reduction. These discrepancies highlight the significant influence of GO source and characteristics on the mechanical performance of cementitious composites. Moreover, while many researchers have reported GO based performance enhancements in concrete [69,70], studies related to GO inclusion in RAC, particularly the effect of GO on ITZs are limited. Sae-Long et al. (2024), also highlighted the significance of investigating the influence of graphene replacement in RAC [14]. Long et al. (2018) investigated the

effect of GO on the ITZ of recycled fine aggregates through SEM imaging, yet the study did not quantitatively assess ITZ composition [71]. In addition, high production cost and CO_2 emissions associated with GO present significant challenges for its widespread adoption in cementitious composites [72,73].

This study aims to address these gaps by employing SEM/EDS mapping to quantify ITZ thickness variations based on elemental composition, specifically focusing on silicon, aluminium, and calcium distributions. Moreover, the effect of GO on the macroscale mechanical properties of RAC is also reported in this study. The comprehensive details included in this study such as the source of graphite, synthesis process, parameters and GO characteristics will enable in-depth understanding and reproducibility of results in this domain. By incorporating GO at optimal dosages, the study aims to improve compressive strength, splitting tensile strength, and elastic modulus of RAC. Through mechanical testing and microstructural analysis, the research outcomes from this study will help develop a novel, industrially applicable strategy to replace a higher fraction of NCA with RCA. This also study presents an economic and environmental assessment, evaluating the cost-effectiveness and sustainability of GO enhanced RAC. This approach provides a more comprehensive understanding of ITZ modifications and industrial applicability of GO induced RAC promoting sustainable practices within the construction industry.

2. Materials and methodology

2.1. Materials

Startup graphite was sourced from Sri Lanka with a particle size distribution of 50–100 μm. Sulphuric acid (98 %), potassium permanganate (99 %), hydrogen peroxide (30 %) and hydrochloric acid (37 %) were purchased from Sigma-Aldrich. Ordinary Portland Cement (OPC) conforming to AS 3972:2010 [74] standards was used as the binder while locally available river sand with a fineness modulus of 3.26 was used as fine aggregates (FA). The water absorption capacity of FA was 0.51 %, tested according to ASTM C128-22 [75]. NCA used in this experiment were crushed granite rock of 20 mm maximum nominal size. A poly-carboxylic ether-based superplasticizer (SP) was incorporated in the mix to improve the workability of concrete. Tap-water was used for all mixing purposes. In addition, laboratory synthesized GO in the form of an aqueous dispersion with a concentration of 10 g/L was used in this study. RCA was obtained from a construction waste recycling company (Alex Fraser Group, Australia) having a nominal maximum size of 20 mm. RCA mainly consisted of old concrete mortar and crushed stone. The water absorption capacity of NCA and RCA were measured in accordance with ASTM C127-24 [76] and recorded as 1.82 % and 5.62 % respectively.

2.2. Methodology

2.2.1. Graphene oxide synthesis and characterization

GO is processed from vein graphite (98 % graphitic carbon) [77], and synthesized according to an improved version of Hummer's method [78]. Initially, graphite powder is soaked in concentrated sulphuric acid for intercalation. Following this treatment, the oxidizing agent, is gradually added into the graphite-acid mixture for oxidation of graphite to graphite-oxide (step I oxidation) for 3 h. Thereafter, the resultant is quenched with a mixture of ice and chilled distilled water (Step II oxidation for 1 h) before complete termination of the chemical reaction by addition of H_2O_2. Finally, the suspension is centrifuged, supernatant decanted and residual is

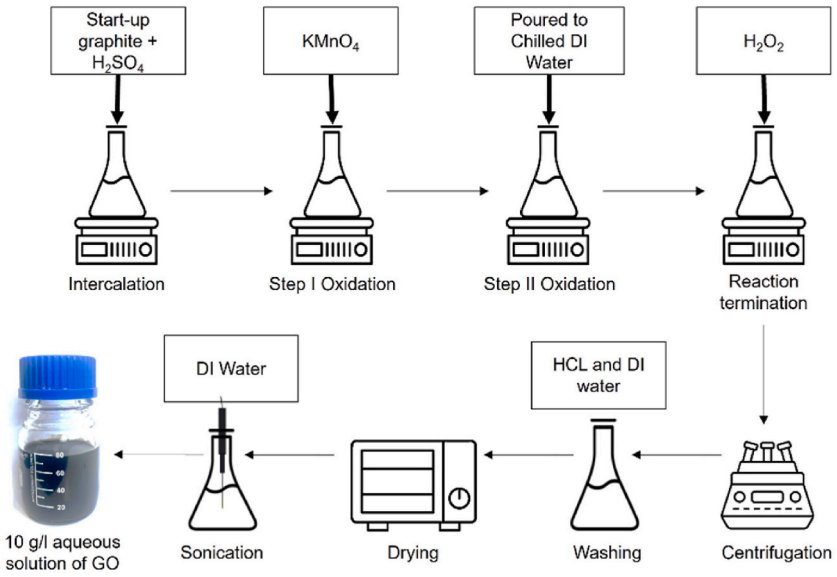

Fig. 2. Schematic illustration of GO synthesis.

proceeded for several washing steps with hydrochloric acid and deionized (DI) water. This step is essential to remove any impurities, unreacted graphite, and residual salts. Thereafter, the resulting semi-solid is oven dried at 50 °C until constant mass to obtain GO powder. Subsequently, a 10 g/L dispersion is prepared using a volumetric method by dispersing 10 g of GO powder in 1 L of DI water. The mixture is sonicated at 30 kHz for 5 min using a probe sonicator (Bioevopeak USCG-1500). It is important to note that sonication was adopted only at this stage of synthesis and Fig. 2 shows a schematic illustration of the synthesis process.

The synthesized GO was then characterized to identify its physical and chemical properties. The surface morphology of GO sheets was examined using SEM (Hitachi FlexSEM 1000 II VP-SEM) and EDS was used to determine the elemental composition. The crystalline structure of GO was investigated by an X-ray diffractometer (XRD; D8 Advance Diffractometer, Bruker). Data was acquired from a 2Θ range of 5–85° at a scan speed of 12°/min with Cu Kα radiation (λ = 1.5406 Å). The chemical identity of GO functional groups was determined by Fourier Transform Infrared spectroscopy (FTIR) on a LUMOS FTIR, Bruker within an infrared radiation range of 800–4000 cm^{-1} at a scan time of 32 scans. In addition, Raman spectra were collected to study the defective ratios of GO. A confocal Raman microscope (inVia Qontor, Renishaw) with a monochromatic light wavelength of 532 nm and spectra range of 1150 cm^{-1} to 3100 cm^{-1} was adopted in the analysis. The thickness of the nanosheets were measured by atomic force microscopy (AFM; Cypher-ES, Asylum Research).

2.2.2. Preparation of RAC mixes and testing

This study adopted a simple mixing procedure ensuring that it can be implemented even in large scale batching plants without the need of sophisticated mixing techniques such as magnetic stirring, high shear mixing, or sonication. Water absorption of RCA (5.62 %) was almost threefold compared to that of NCA (1.82 %) owing to high volume of adhered mortar. Therefore, to minimize the effect on test results, RCAs were brought to saturated surface dry (SSD) condition before casting concrete. Initially, RCAs were fully immersed in water for 24 h and subsequently dried for another 24 h to reach SSD condition. Prior to mixing with the solid materials (cement, FA, RCA and/or NCA), the liquid content was prepared by manually stirring the SP, water and 10 g/L GO dispersion for 30 s using a glass rod of 8 mm diameter. This was done to leverage the steric hindrance behaviour of SP to effectively disperse GO [79] in the liquid content and subsequently in the cement matrix. Thereafter, the liquid content was directly added to the solid mix and concrete was mixed as per AS 1012.2:2014 [80]. The mixing procedure of GO induced RAC is schematically illustrated in Fig. 3.

Proceeding the mixing process, the concrete mixes were poured into cylindrical molds (100 mm dia. x 200 mm height) and compacted using a vibrating table. Table 1 presents the detailed mix proportions of the five concrete batches that were casted. Mix ID "100NCA" represents conventional concrete comprising entirely of (100 %) NCA, whereas "0GO" represents RAC with 50 % NCA, and 50 % RCA. Correspondingly, "0.015GO", "0.035GO" and "0.065GO" represent RAC (50 % NCA,50 % RCA) containing GO in dosages of 0.015 %, 0.035 % and 0.065 % bwoc respectively.

In each of the concrete batches, the resultant water/cement ratio was maintained at 0.4 by requisite adjustments for moisture content and water absorption in aggregates. The specimens were demolded after 24 h and cured in a standard water bath until testing. Fresh properties of the RACs, were assessed through slump tests (AS 1012.3.1 [81]), and the mechanical strengths through compressive strength, split tensile, and elastic modulus tests (AS 1012.9:2014 [82]). The microstructure of the composites including the ITZs were examined through SEM analysis at 28 days for the 0GO and 0.035GO specimens.

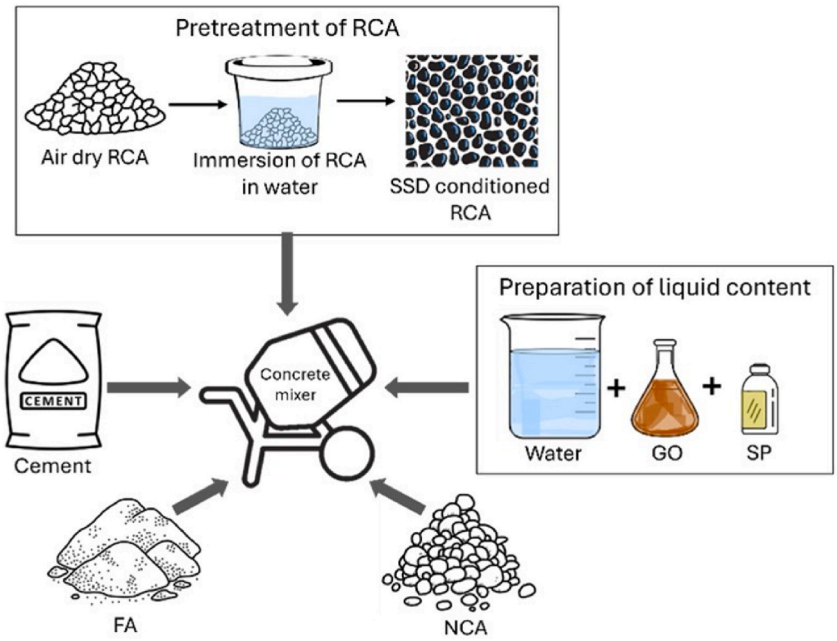

Fig. 3. Mixing process of GO induced RAC.

Table 1
Mix proportions of concrete mixes (kg/m^3).

Mix ID	Cement	NCA	RCA	FA	SP	Water	GO
100NCA	450	1087	–	563	2.205	180	–
0GO	450	543.5	543.5	563	2.205	180	–
0.015GO	450	543.5	543.5	563	2.205	180	0.0675
0.035GO	450	543.5	543.5	563	2.205	180	0.1575
0.065GO	450	543.5	543.5	563	2.205	180	0.2925

Note: NCA-natural coarse aggregates; RCA-recycled concrete aggregates; FA-fine aggregates; SP-superplasticizer; GO- graphene oxide.

Subsequently, a comparative environmental and cost analysis was conducted on the investigated concrete mixes. The environmental assessment focused on the embodied carbon footprint from cradle to gate, corresponding to stages A1-A3 in EN 15978:2011 [83], with CO_2 emissions expressed in kg CO_2-equivalent. The CO_2 emissions inventory was primarily sourced from the latest EPiC Database [84], which compiles processed data from the Australian Life Cycle Inventory Database Initiative (AusLCI) [85]. Unit prices were obtained from multiple sources, including recent retailer quotes and relevant publications within the Australian context. The CO_2 emissions and unit cost inventory for all materials are summarized in Table 2. It is important to note that the scope of the environmental and cost analysis in this study is specific to the Australian context.

Since CO_2 emission or cost alone may not comprehensively reflect the economic and environmental impacts, two indices; C_I (cost index in AUD/MPa) and E_I (CO_2 emission index in $kgCO_{2\text{-eq}}$/MPa) were employed to evaluate and compare the overall performances of the concrete mixes according to Eqn. (1) and Eqn. (2) respectively [94,95].

$$C_I = \frac{\sum Cost}{f_c} \quad \text{Equation 1}$$

$$E_I = \frac{\sum Embodied\ Carbon}{f_c} \quad \text{Equation 2}$$

Where $\sum$Cost is the total cost per m^3 of concrete (AUD), f_c is the compressive strength of the corresponding concrete mix at 28 days (MPa), and $\sum$Embodied Carbon is the total carbon dioxide emissions ($kgCO_{2\text{-eq}}$) per m^3 of concrete.

3. Results and discussion

3.1. Characterization of GO

Surface morphology of GO was studied by optical microscopy and SEM while the degree of oxidation was assessed by EDS analysis. The size distribution of GO sheets was obtained by measuring more than 50 individual sheets in the sample. According to the SEM and optical microscopic images, the average size of GO sheets is widely distributed from about ~8 μm–40 μm in the dispersion. Fig. 4a illustrates the distribution of sheets on a glass slide as observed under a microscope. A thin lamellar structure of GO with wrinkled surface features are observed through SEM analysis as presented in Fig. 4b. This is a common observation in chemically converted monolayer or few layer GO sheets [96]. A recent study has revealed that the wrinkled surface texture enhances the interlocking between the cement matrix and the 2D nanomaterial and thereby, improving the overall composite strength [97].

Fig. 5a, b and 5c shows the region analysed, spectrum obtained, and the elemental composition of GO, respectively. The EDS analysis demonstrate that a major proportion of the material consist of carbon and oxygen while trace amounts of other impurities such as nitrogen, sulphur, and chlorine are also present. The high oxygen content signifies the successful conversion of graphite to GO. Moreover, this observation proves the incorporation of oxygenated functional groups on the surface of GO.

From the analysis, the Carbon to Oxygen ratio (C/O) is calculated as 1.73 indicating a strong oxidation level. GO derives its hydrophilicity from oxygen-containing functional groups and thereby these results prove the ease of dispersibility of GO in water [98]. This constitutes a significant benefit of employing GO in cementitious composites, as it can be easily blended with mixing water during the concrete batching process without the need for additional dispersants and complicated procedures.

Fig. 6 represents the XRD diffractogram of GO and it exhibits a distinct diffraction peak at $2\Theta = 10.199^\circ$ which corresponds to the

Table 2
CO_2 emissions and unit cost of raw materials.

Material	CO_2 emissions ($kgCO_{2\text{-eq}}$)	Cost per kg (AUD)
Cement	0.885 [86]	0.2 [86]
NCA	0.036 [87]	0.06 [86]
RCA	0.008 [88]	0.02 [86]
FA	0.024 [89]	0.05 [86]
SP	4.610 [90]	2.9 [90]
Water	0.001 [91]	0.005 [86]
GO	23.2 [92]	200 [93]

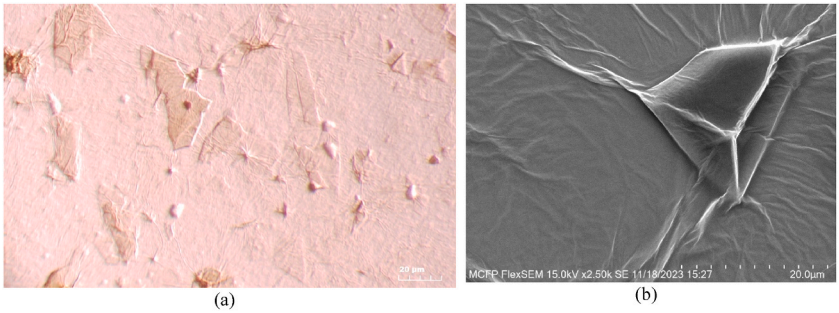

(a) (b)

Fig. 4. Images of GO sheets through (a) optical microscopy, (b) scanning electron microscopy.

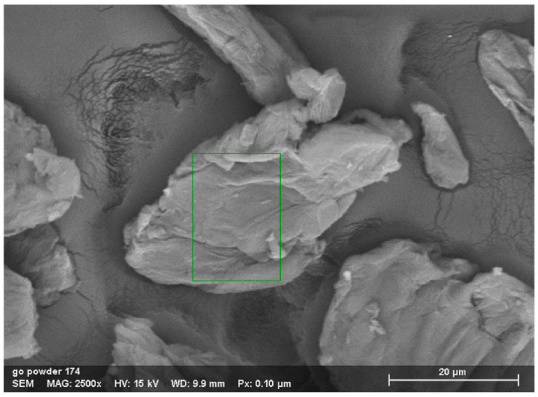

(a)

Element	%
C	60.21
O	34.87
S	1.17
N	2.96
Cl	0.30
Cu	0.49
Total	100.00

(c)

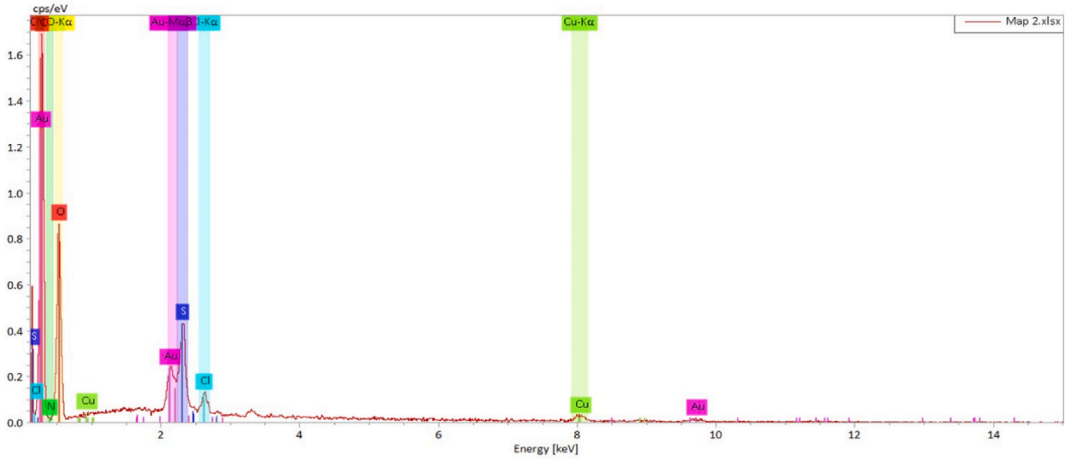

(b)

Fig. 5. SEM/EDX analysis (a) SEM of GO sheet, (b) EDX spectrum, (c)elemental composition of GO.

reflex from (001) plane. The interplanar distance of the most intense peak was calculated using Bragg's Law (Eqn. (3)):

$$n\lambda = 2dsin\Theta \quad \text{Equation 3}$$

where "n" is an integer, "λ" is the wavelength of Cu source (λ = 1.5406 Å), "d" is the d-spacing and "Θ" is the scattering angle. The XRD spectra resemble an interlayer spacing (d) of 8.66 Å which indicates a much larger interplanar distance compared to feedstock graphite (d = 3.35 Å) [99]. This is due to the expansion of graphitic interlayer spaces during the intercalation and oxidation stages in the synthesis process which has a direct positive relationship to the degree of oxidation and amount of intercalated water molecules. The XRD results from this study are in good agreement with previous literature [100,101]. The other two minor peaks at 2Θ = 20.402° and 42.344° arise from (002) and (100) planes respectively [102]. This finding is further supported by the results of Dahanayake et al.

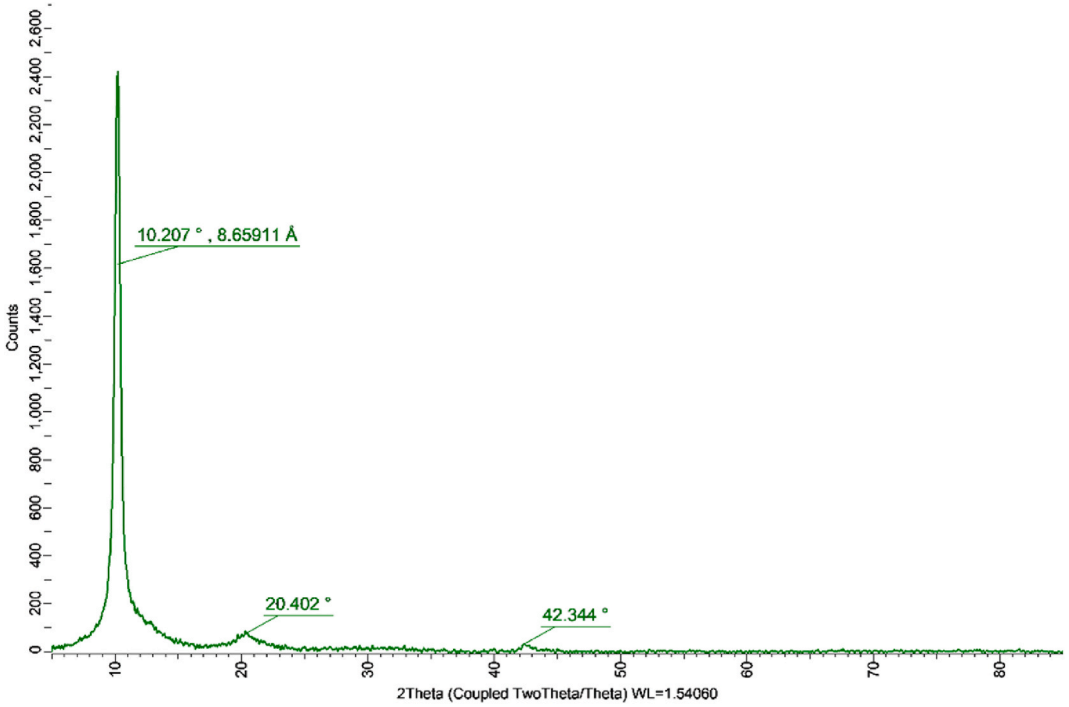

Fig. 6. XRD spectra of GO.

[103] which used the same startup graphite source. The interlayer spacing of GO for cementitious composites is an important characteristic as the entrapped interlayer water can serve as an alternative water reservoir for self-curing at later stages of hydration [104].

Fig. 7 represents the FTIR spectrum of GO used in this study including the different types of oxygenated functional groups. The broad absorption band at ~3500-2500 cm^{-1} originates from the stretching modes of O-H bonds such as tertiary alcohols and interlayer adsorbed water molecules [100]. The 1720 cm^{-1} band is assigned to carbonyl stretching modes carboxylic acids, ketone, or ester groups. Moreover, the major peak at 1618 cm^{-1} corresponds to the stretching vibrational mode of aromatic C=C groups while the

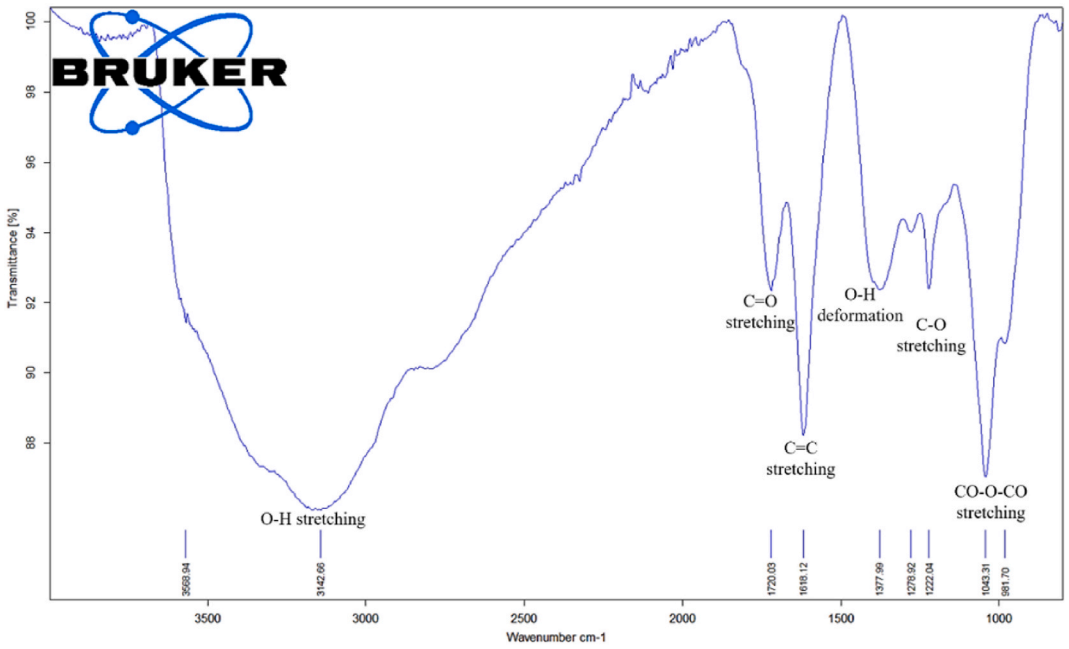

Fig. 7. FTIR spectrum of GO.

bands at 1377 cm^{-1} and 1222 cm^{-1} have been traditionally assigned to bending of tertiary C-OH groups and epoxide functional groups respectively [105].

This further confirms the presence and identity of oxygenated functional groups in GO. These chemically active groups undergo reactions with un-hydrated cement (alite, belite and tricalcium aluminate) increasing nucleation sites for hydrated products such as calcium silicate hydrate [106]. Previous studies evaluating the relationship between functional groups and strength enhancement in GO-concrete concluded that the edge-plane carboxyl (-COOH) groups form strong covalent bonds with hydrated calcium silicates increasing the interfacial bonding between the cement matrix and GO [107]. Furthermore, a molecular dynamics model by Hou et al., established that most of the COOH groups deprotonate and bond with adjacent Ca^{2+} ions in the system to form stable COO-Ca bonds via strong covalent bonding [108].

The Raman spectrum of GO used in this study is shown in Fig. 8. The spectra highlight three characteristic peaks associated with defective and graphitic behaviour of GO. The first peak at 1352 cm^{-1} (D-band) evolves due to defects in the carbon lattice. These defects can be described as structural defects (holes) due to oxidation such as misarrangement of the six-membered lattice or due to chemical functionalization hybridising the sp^2 carbon atoms to sp^3 state [109]. The G-band at 1598 cm^{-1} is derived from C-C stretching of sp^2 carbon atoms in the lattice and can also be associated with the defects in the edge plane [110]. The broad 2D band at 2685 cm^{-1} is due to the overtone of Raman-active groups and its intensity decrease with defects. Furthermore, the defect ratio (I_D/I_G) is frequently used to assess the degree of disorder of carbon-based materials. The I_D/I_G of the GO used in this study was found to be 0.81. This observation indicates the existence of sp^3 defects within the sp^2 carbon lattice, signifying chemical functionalization of GO [111].

The morphology including the thickness of GO was also studied using AFM. Fig. 9 demonstrates the sheets analysed and the 2D height profile of two GO sheets in the vicinity. The thickness (d_z) of the two sheets were found to be consistent with an average of 1.38 nm despite the change in lateral size. These results are consistent with earlier studies which also conclude that the thickness of a single GO sheet lies in the range of 1–1.5 nm irrespective of the synthesis process, and startup graphite particle size [112,113].

3.2. *Influence of GO on the workability of RAC*

The workability of the fresh concrete was evaluated using the slump test, with the average slump values for different mixtures presented in Fig. 10. To ensure accuracy and minimize experimental errors, each mix was tested three times, and the average value is reported. Although RCA possess about three times higher water absorption than NCA due to high volumes of old adhered mortar around the aggregate, pre-saturation of RCA in water for 24 h eliminates loss of workability due to absorption of free water and saturation of RCA. Since RCA was used in SSD condition, replacing 50 % of NA had no adverse effect on the workability. This is consistent with current literature that has evaluated the pre-saturation strategies to overcome workability issues associated with RCA [114,115]. However, from Fig. 10, it is evident that incorporation of increased dosages of GO (0.035 % and 0.065 %) into the concrete mix led to about 36 % and 45 % decrease in workability respectively. This can be attributed to the hydrophilic behaviour of GO due to the abundant oxygenated functional groups.

As GO is functionalized with oxygenated groups (evident from nanomaterial characterizations above) with a very high surface area, it has high affinity towards water molecules. Therefore, it absorbs water molecules and reduces the workability of concrete. This

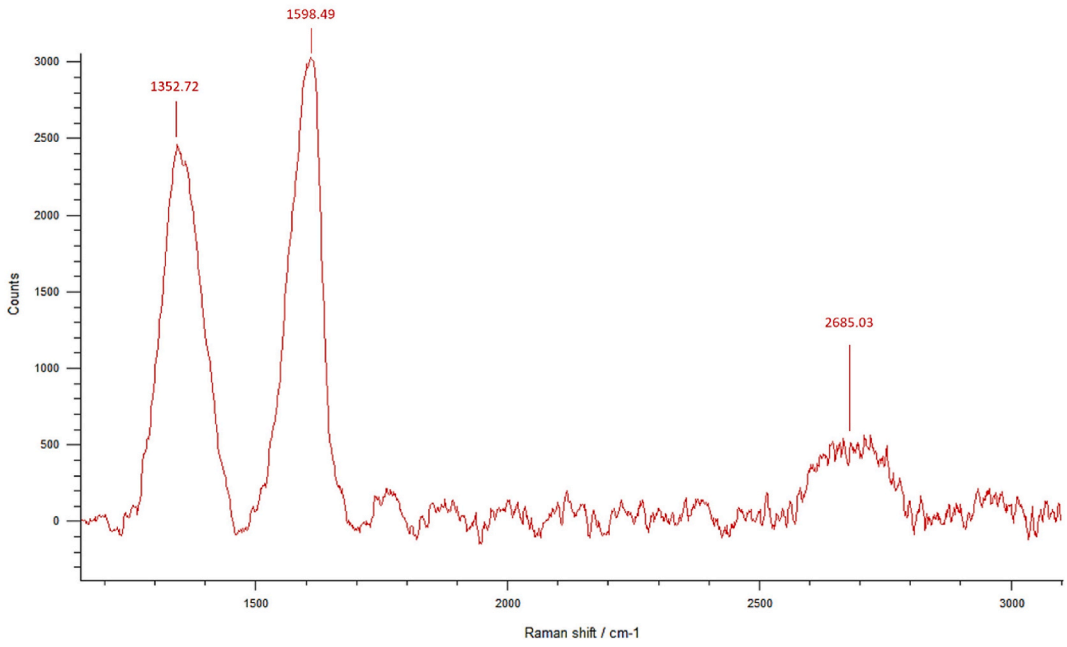

Fig. 8. Raman spectra of GO.

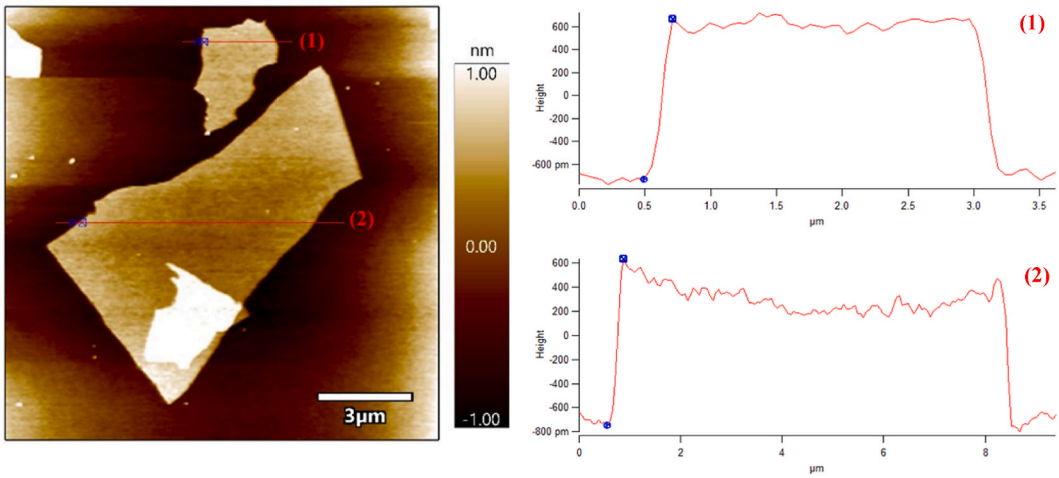

Fig. 9. AFM image with height profiles of two sheets.

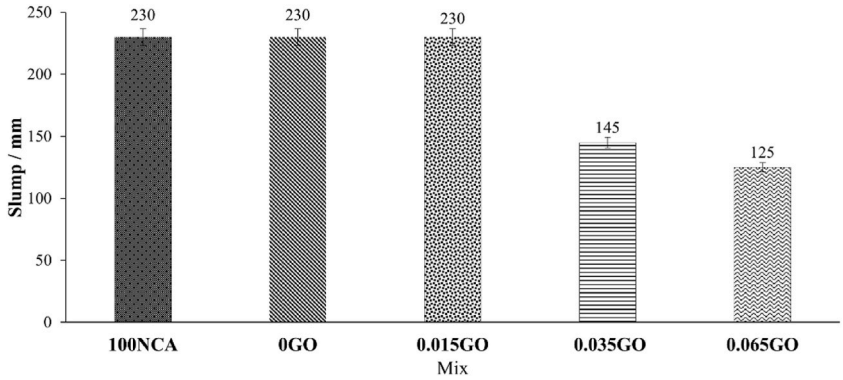

Fig. 10. Workability of different concrete mixes.

observation is comparable with previous research which reported that the addition of GO diminishes the fluidity of concrete due to entrapment of water by GO [116,117]. However, this workability reduction can be averted by incorporating additives such as viscosity modifying agents or addition of mineral admixtures such as fly ash, or slag [118,119].

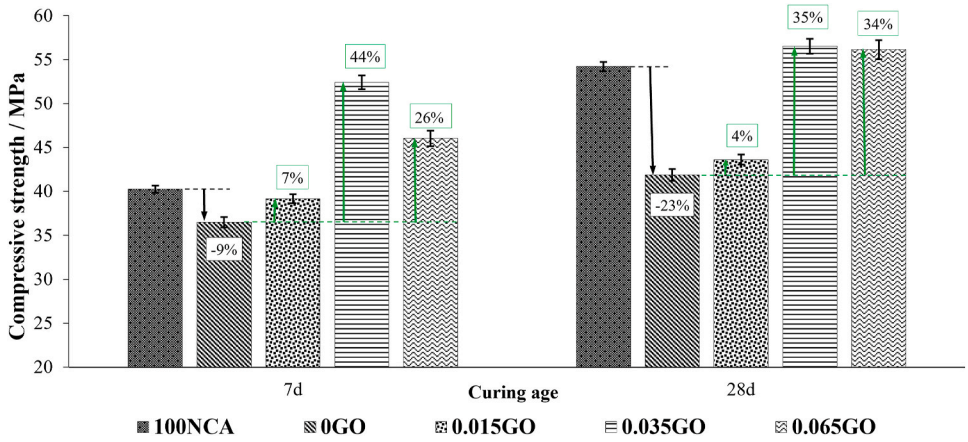

Fig. 11. Compressive strength of concrete mixes.

3.3. Influence of GO on mechanical performance of RAC

Mechanical performances of the RAC mixes were comprehensively evaluated through compressive strength, splitting tensile strength, and elastic modulus tests at 7 and 28 days of curing. For each mechanical test, the reported results represent the average values obtained from three specimens and the corresponding standard deviations are included in the figures to illustrate data variability. Additionally, samples were visually examined to assess failure patterns, providing a holistic understanding of the influence of GO on RAC.

Fig. 11 illustrates the results of compressive strength tests conducted as per ASTM C39 standards [120]. The percentage reduction in compressive strength due to RCA replacement (relative to 100NCA concrete) and the enhancement from GO addition (relative to 0GO concrete) are also highlighted in Fig. 11. It is evident that partial substitution of NCA with RCA lead to a decrease in compressive strength by 9.3 % and 22.7 % at 7 and 28 days respectively. This finding is consistent with that of Chang et al. (2022) which reported a 19 % compressive strength reduction in Grade 50 concrete containing 50 % RCA and 50 % NCA (with respect to 100 % NCA concrete) at 28 days [121]. In general, the degree of strength loss correlates to the fraction of RCA used in the mix [122]. In a research study by El-Hassan et al. (2019), total replacement of NCA with RCA led to a detrimental compressive strength reduction of 87 % [123]. Furthermore, Tam et al. reviewed that complete replacement of NCA degrades the compressive strength of RAC by about 40 % [38]. This is attributed to the porous residual mortar in RCA and the three weak ITZs in RAC compared to that of conventional concrete which significantly compromises the mechanical integrity of RAC [13].

However, inclusion of GO showed a distinct impact to the compressive strength of RAC specimens. As presented in Fig. 11, compressive strength of RAC with GO (0.015GO, 0.035GO and 0.065GO) was higher than that of RAC without GO (0GO). Compared to 0GO, the compressive strengths of 0.015GO, 0.035GO and 0.065GO were increased by 7.3 %, 43.6 % and 26.1 % respectively at 7 days. Similarly, at 28 days, the strength gains of 0.015GO, 0.035GO and 0.065GO increased by 4.2 %, 35.0 % and 34.0 % respectively. It is evident that for both 0.015GO and 0.035GO, the early age strength gain is more significant than the 28-day strength gain. In the early stages of curing, GO provides additional nucleation sites for cement hydration through its oxygenated functional groups, thereby accelerating the hydration process and contributing to a denser microstructure [124]. However, as curing progresses, the chemical environment in the cement matrix changes gradually (decrease in active and free Ca^{2+} ions) to form hydrated products. This can potentially lead to a reduced interaction of cement particles and GO with time.

The failure mechanisms of RAC specimens were assessed to understand the influence of GO on fracture behaviour under compression. Specifically, specimens with the highest and lowest 28-day compressive strengths (0.035GO and 0GO) were analysed after fracture. According to ASTM C39/C39M, common fracture modes in cylindrical concrete specimens under compressive loading include vertical cracking, cone-and-split failures, and shear planes. In this study, both concrete types exhibited columnar vertical cracking that extended through both ends of the cylinders, as illustrated in Fig. 12a and b. For all tested specimens, a gradual formation of surface cracks was observed until the point of failure. Despite the significant difference in compressive strength, the observations indicate that while the macro-scale fracture mechanisms remain unchanged, the nano-scale enhancements facilitated by GO significantly contribute to the improved compressive capacity of RAC. These results highlight the potential of GO as a nano-modifier to mitigate the inherent weaknesses of RCA, paving the way for the development of high-performance sustainable concretes. Further microstructural analyses in subsequent sections provide additional validations of these observations.

Consistent with the trends observed for compressive strength, the RAC samples containing GO exhibited higher splitting tensile strength and elastic modulus compared to the control sample without GO as shown in Fig. 13a and b. The partial replacement of NCA with RCA resulted in a significant reduction in splitting tensile strength by 6.3 % and 15.8 % at 7 and 28 days, respectively. However, 0.035GO demonstrated a 27.6 % improvement in splitting tensile strength compared to 0GO at 28 days. Notably, it also surpassed the splitting tensile strength of the benchmark sample (100NCA) by 19 % at 7 days and 3 % at 28 days. Previous studies have highlighted

(a) (b)

Fig. 12. Failure patterns of (a)0GO and (b)0.035GO.

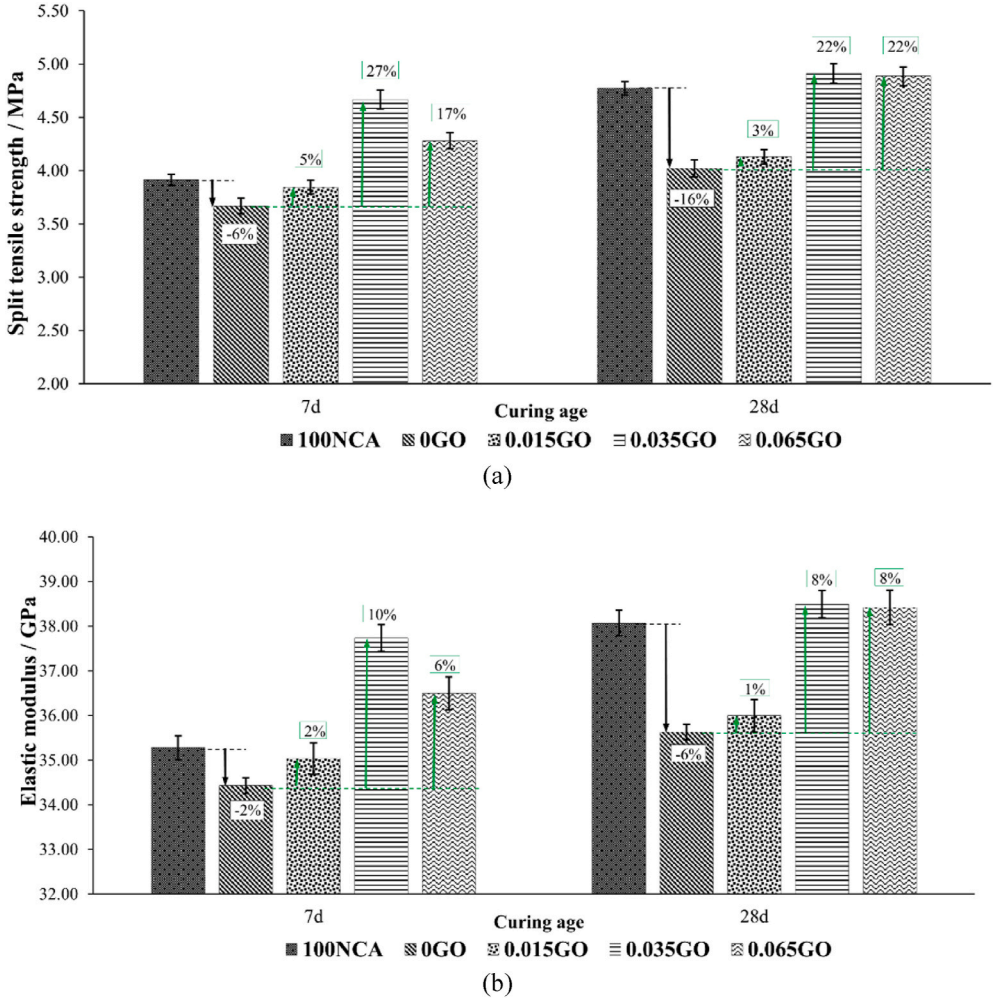

Fig. 13. (a) Splitting tensile strength (b) Elastic moduli of 100NCA, 0GO and 0.035GO.

that splitting tensile strength is influenced by the microhardness of the ITZ and the bonding strength between aggregates and the cementitious matrix [125,126]. The chemical interaction between functional groups of GO and cement particles increases the degree of hydration, which densifies the microstructure of cement paste and strengthens the ITZ between aggregates and cement matrix [127].

Similar to the trends observed in compressive strength and split tensile strength, the highest improvement in elastic modulus was observed in 0.035GO (Fig. 13b) which denotes the consistent enhancement in mechanical performance. Partial replacement of NCA with RCA reduces the elastic modulus by 6.41 % at 28 days, highlighting the detrimental impact of RCA on concrete stiffness. However, 0.035GO specimens demonstrated 9.6 % and 8.0 % improvements in elastic modulus (compared to the control) at 7 and 28 days, respectively. Particularly, at 7 days the elastic modulus of 0.03GO was 7 % higher than the benchmark mix (100NCA). In general, the modulus of elasticity of concrete is influenced by aggregate quality, concrete grade, and the characteristics of ITZ [128–130]. These findings are consistent with previous studies reporting a 3–10 % improvement in the elastic modulus of concrete with minor GO additions [131–134]. The results confirm that GO can effectively counteract the mechanical deficiencies associated with RCA, enhancing the compressive, splitting tensile and elastic moduli. These observations are further supported by the microstructural analysis, which reveals a reduction in microcracks and ITZ widths in the GO enhanced RAC samples.

In addition, it should be noted that the strength enhancement is not linear with the dosage of GO but rather presenting an optimal content. The optimum dosage of GO to deliver the maximum mechanical performance is identified as 0.035 % bwoc. Interestingly, introducing GO beyond its optimum dosage does not further enhance mechanical properties as evident from the test results of 0.065GO specimens in compressive strength, splitting tensile strength and elastic modulus. This is partially attributed to the loss of packing density due to poor workability of 0.065GO mix [135]. Moreover, the high surface area and surface energy of GO at higher dosages promote agglomeration in alkaline cementitious environments, reducing dispersion efficiency within the cement matrix and consequently diminishing its strengthening effects [136]. These outcomes are consistent with previous studies which conclude that GO dosages beyond ~0.05 % bwoc impede the effectiveness of dispersibility and hydration in cementitious composites [137,138].

Re-engineering RCAs by incorporating GO is emerging as a research hotspot amongst many scholars [139–141]. Qidong et al.

(2022), investigated the differential impact of GO to enhance the ITZ of RAC. The findings conclude that addition of 0.05 % GO bwoc enhances the compressive strength by about 20 % at 28 days [142]. In a more recent study by Lu et al. (2023), GO coated RCA were used to enhance the ITZ in concrete where several complicated treatment and mixing procedures were adopted in their study including amino functionalization and nanocoating. GO-soaked RCA was considered as the most effective solution yielding a 25.3 % strength enhancement at 28 days [143]. However, the novelty of the current research stands in the simplicity and industrial applicability of the adopted methodology to achieve a significant strength enhancement (up to 44 %) in GO induced RAC equivalent to conventional concrete (100NCA). The manual addition of pre-mixed 10 g/L GO dispersion into the total liquid content introduced in this paper streamlines the mixing process, ensuring feasibility at an industrial scale. GO dispersions are commonly enhanced through prolonged sonication and shear mixing. However, excessive processing of GO and SP mixtures can lead to polymer chain degradations [61], adversely affecting workability and hydration kinetics in cementitious composites. In addition, Liu et al. (2021) claim that prolonged sonication (30 min) and intensive sonication powers destroy the lamellar structure of GO compromising the dispersibility [144]. Similarly, Rios et al. (2024) also conclude that the sonication time and energy alter the dimensions of GO sheets impacting the mechanical properties and porosity of the cementitious composites [145]. This study achieves effective dispersibility of GO in the 10 g/L aqueous dispersion by adopting a short sonication time (5 min) and power of 30 kHz. The effectiveness of the adopted dispersion technique and concrete mixing method is further supported by the mechanical test results, where the standard deviation was well below 2 %. This indicates uniform distribution of GO within the cementitious matrix, minimizing localized clustering that often compromises material performance. For straightforward adoption in the construction industry, GO dispersion techniques must align with conventional concrete batching processes. In this study, sonication was applied only during the synthesis process, eliminating the need for sophisticated infrastructure changes at batching plants to mix GO in concrete. While methods such as surfactant-assisted dispersion and prolonged ultrasonication require additional processing steps and specialized equipment, the methodology proposed in this study can seamlessly integrate into existing workflows.

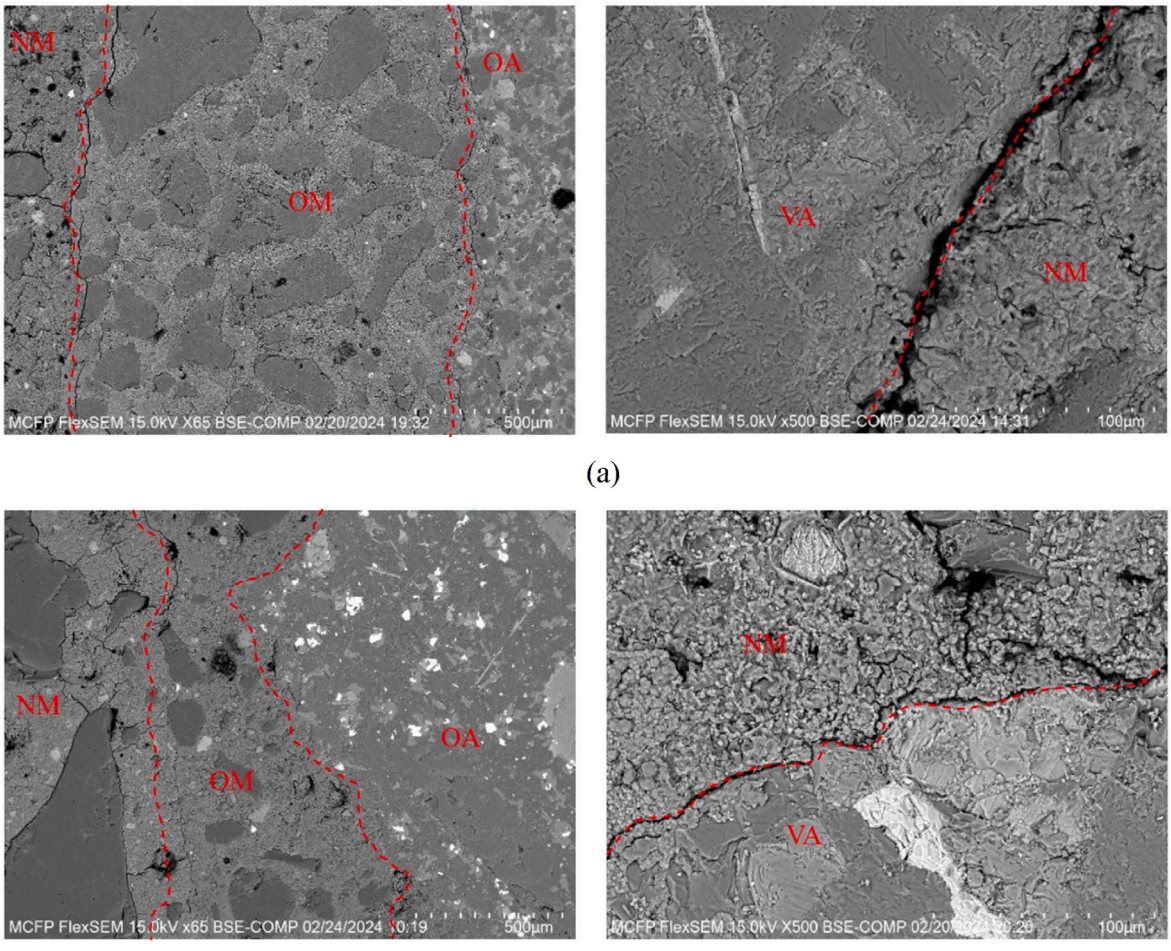

Fig. 14. Typical SEM images of ITZs in (a) 0GO and (b)0.035GO.

3.4. Microstructural analysis and ITZ

The microstructure and ITZs of control mix (0GO) and 0.035GO were investigated using SEM. The elemental distributions were tested by EDS mapping after curing the concrete samples for 28 days. Low-magnification SEM images were captured to clearly identify

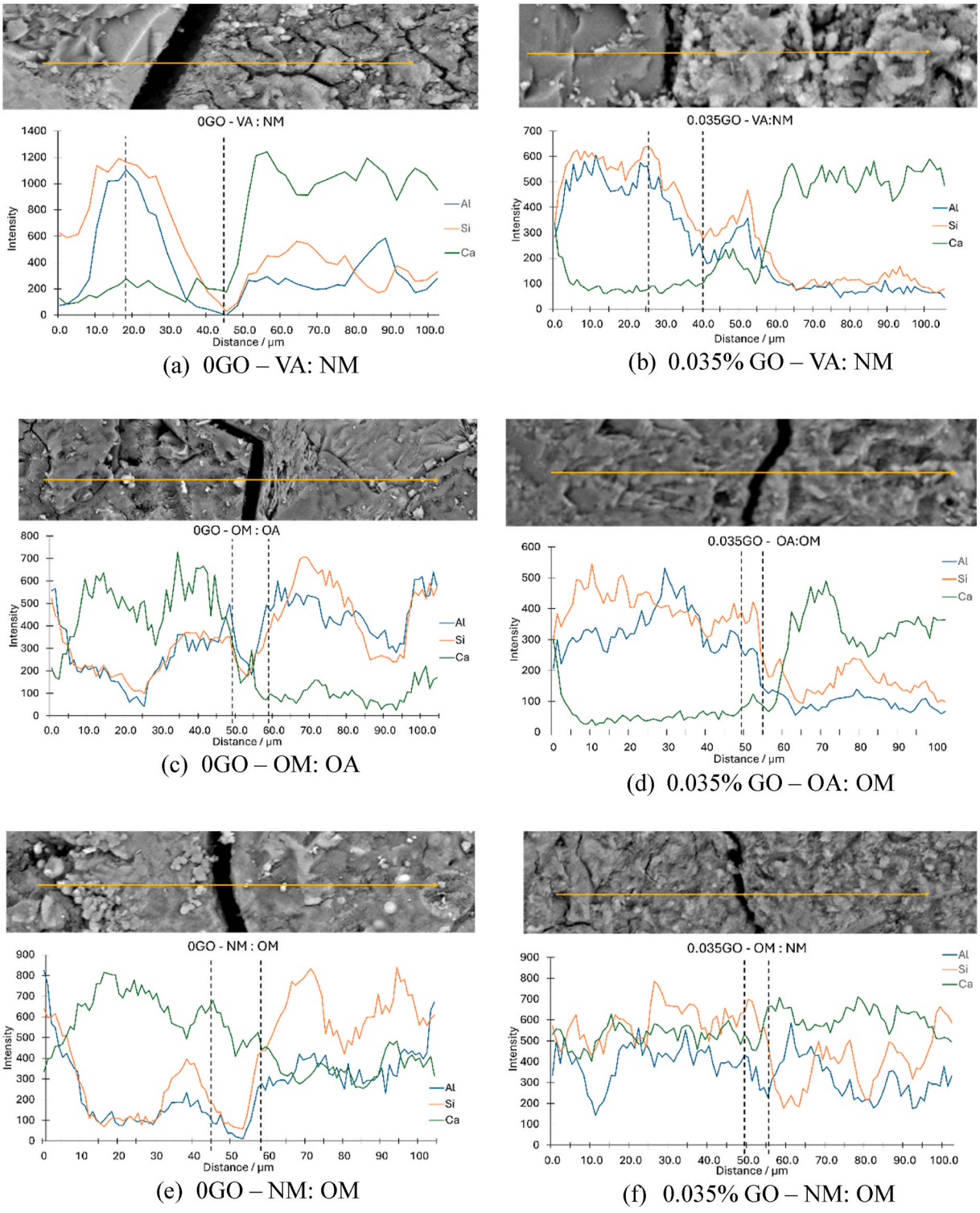

Fig. 15. EDS line scan maps across virgin aggregate (VA), new mortar (NM), old mortar (OM), old aggregate (OA).

the four main sections: interfaces between the old-adhered mortar (OM), new mortar (NM), old aggregate (OA) and virgin aggregate (VA) in RAC as illustrated in Fig. 14. High magnification Back Scattered Electron (BSE) mode was adopted for line scan mapping.

Line scan mapping was employed to determine the thicknesses of ITZs by examining variations in the quantities of three main elements (Ca, Si, and Al). Since the samples were composed of the same materials and both NCA and RCA are granite (with high Si and Al content), the levels of Si and Al in the aggregate phase exhibited significant fluctuations, gradually decreasing upon reaching the ITZ, and stabilizing at lower levels in the cement mortar phase. Contrastingly, the trend for Ca was the opposite due to the use of OPC, which has a high Ca content. The intensity of the Ca element was low in the aggregate phase, increased through the ITZ, and stabilized at higher levels in the cement matrix. This pattern facilitates a clear differentiation between aggregate and cement matrices in the concrete. However, distinguishing between old mortar and new mortar using elemental line scans is challenging because both components have high Ca content. Therefore, low-magnification imaging and a built-in camera navigation system was utilized to effectively differentiate these two sections. Fig. 15 demonstrates the line scan maps and changes in element content which directly reflects the width of ITZs. According to the elemental change, the width of the VA: NM ITZ (Fig. 15a) is approximately 25 μm, which decreased to ~15 μm (Fig. 15b) due the addition of GO. This implies a significant effect of GO to enhance the newly formed ITZ of RAC. In terms of OM: OA ITZ (Fig. 15c), the thickness is in the range of 15–20 μm, which is 5–10 μm wider than the ITZ of 0.035GO (Fig. 15d). Moreover, Figs. 15e and f compare the ITZ widths between the OM and NM in the 0GO and 0.035GO samples respectively. In comparison to the 0GO sample, width of OM: NM ITZ of 0.035GO has also decreased by approximately 40–50 %. Therefore, these findings suggest that the addition of GO in RAC enhances the ITZ properties at nano and microstructural levels which results in the improvement of macroscale characteristics.

The relationship between the addition of GO and improvement of ITZs can be explained in terms of the strength gain mechanisms associated with GO and cement. The oxygenated functional groups of GO are highly reactive in chemical environments. In addition, cement also has chemically reactive ions such as $Ca^{2+}$and Al^{3+} ions in clinker. GO nanosheets are adsorbed onto cement grains, where their oxygenated functional groups facilitate chemical and interfacial bonding with Ca^{2+} ions in calcium silicate hydrate (CSH) and calcium hydroxide (CH) phases. Specifically, hydroxyl (-OH), carbonyl (-C=O), and carboxyl (-COOH) groups in GO interact with Ca^{2+} ions, enhancing chemical adhesion between hydration products and GO lamellae. This interaction contributes to a more cohesive and densified microstructure, thereby improving the mechanical performance of the composite [146]. This leads to an improvement in the degree of hydration around the ITZ [147]. The SEM images in Fig. 15a and b, further demonstrate that the cement matrix with GO has relatively fewer microcracks compared to the control sample. Furthermore, the physical properties of GO such as high tensile strength and elastic modulus can also restrain the initiation of cracks. In addition, due to strong CSH-GO bonding, cracks tend to deflect GO densified phases and propagate along weaker regions in the cement matrix. Since the ITZs are the weakest links in RAC, the microstructural enhancements in these regions are imminent to recover the performance loss and increase the percentage inclusion of RCA in concrete.

3.5. Economic and environmental evaluation

Since GO induced RAC showed desirable enhancements in both mechanical and microstructural properties, an economic and environmental analysis considering the cost and CO_2 emissions was conducted to assess the feasibility of introducing GO as a performance enhancer. Fig. 16a and b summarizes the calculated results of the cost index (C_I) and CO_2 emissions index (E_I) of the five concrete mixes used in this study.

The C_I for conventional concrete (100NCA) is 3.52 AUD/MPa, while the control mix (0GO) exhibits a higher C_I of 4.03 AUD/MPa, reflecting RAC's lower mechanical strength. Incorporating 0.035 % GO reduces the C_I to 3.55 AUD/MPa, closely aligning with 100NCA while significantly enhancing microstructural integrity and compressive strength. However, other GO dosages (0.015 % GO at 4.18 AUD/MPa and 0.065 % GO at 4.05 AUD/MPa) result in higher costs, likely due to insufficient GO content at lower dosages and agglomeration effects at higher dosages. Thus, 0.035 % GO is identified as the most cost-effective option for practical applications.

The E_I for 100NCA is 8.51 $kgCO_{2\text{-eq}}$/MPa, while the 0GO mix increases to 10.65 $kgCO_{2\text{-eq}}$/MPa, indicating that RCA alone does not effectively reduce CO_2 emissions due to inferior mechanical properties (lower MPa values). However, at an optimal 0.035 % GO dosage, E_I reduces to 7.95 $kgCO_{2\text{-eq}}$/MPa, demonstrating the potential of GO to enhance strength and lower CO_2 emissions per unit strength.

Beyond the direct economic and environmental considerations, GO-enhanced RAC offers additional benefits that further justify its use. As reported in this study, GO densifies the microstructure and enhances the ITZ of RAC. These improvements can lead to enhanced durability, resistance against aggressive exposure conditions and water permeability [42,148] which increases the service life of structures and reduce maintenance [149]. Furthermore, with the growing demand for graphene materials, the cost of GO is expected to decline as production volumes increase [150]. This reduction in cost will improve the economic feasibility of incorporating GO in the concrete industry, making its large-scale application more viable and will drive significant advancements in eco-efficient and high-performance concrete.

4. Conclusions and future recommendations

This study provides comprehensive insights into the effects of GO on the workability, compressive strength, splitting tensile elastic moduli, ITZ and microstructural properties of RAC. GO was admixed in three different dosages of 0.015 %, 0.035 % and 0.065 % bwoc to concrete containing 50 % RCA. Based on these examinations, the following conclusions can be drawn:

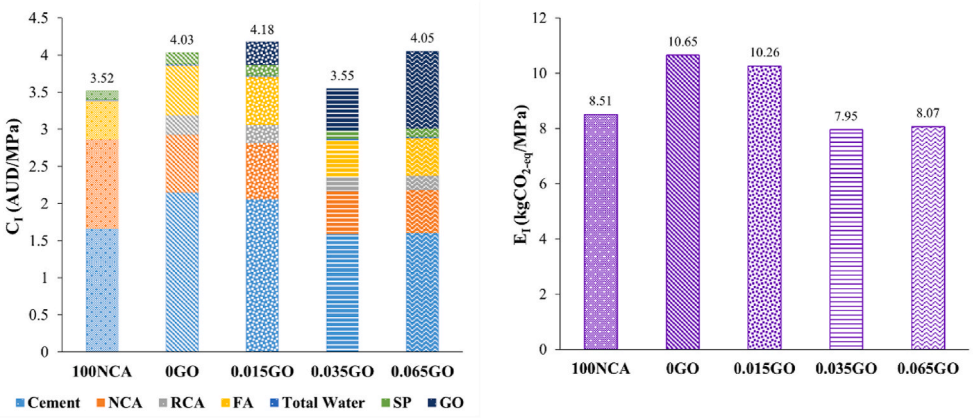

Fig. 16. (a) Cost and (b) CO_2 emission index of concrete mixes.

1) Replacing 50 % of NCA with RCA in SSD condition effectively mitigated the adverse impact on workability. However, the addition of higher dosages of GO at 0.035 % and 0.065 % bwoc resulted in significant decreases in workability by approximately 36 % and 45 %, respectively due to the high-water affinity of GO functional groups.
2) Partial replacement of NCA with RCA reduced compressive strength by up to 22.7 % at 28 days. However, incorporating GO at an optimal dosage of 0.035 % bwoc enhanced the compressive strength of RAC beyond the benchmark (100 % NCA) mix. Specifically, a 35 % strength improvement was observed at 28 days, making the GO-RAC mix a viable alternative to conventional concrete.
3) 0.035 %GO-treated RAC exhibited superior splitting tensile strength and elastic modulus compared to both the control and benchmark mixes. At 28 days, the tensile strength increased by 27.6 % compared to the control, and the elastic modulus showed a 9.6 % improvement, highlighting GO's ability to enhance concrete stiffness and resistance to cracking.
4) From the microstructural evaluation of the ITZs by SEM and line scan mapping by EDS, it can be concluded that the widths of ITZs between VA: NM, OA: OM, and OM: NM decreased by ~15 μm, ~10 μm and ~5 μm respectively with the addition of 0.035 % GO.
5) The enhancement in macroscale properties and microscale characteristics in GO-RAC can be attributed to promoted nucleation effect, densified microstructure, and mitigation of crack propagation in the cement matrix and the ITZ.
6) Among all tested GO dosages, 0.035 % GO was the most cost-effective and sustainable option, with a C_I of 3.55 AUD/MPa and an E_I of 7.95 $kgCO_{2-eq}$/MPa. These values are comparable to those of conventional concrete (100NCA: 3.52 AUD/MPa, 8.51 $kgCO_{2-eq}$/MPa), indicating that 0.035 % GO can achieve similar economic and environmental performance while enhancing mechanical properties.

This research highlights the transformative potential of GO as a nano-modifier for RAC. By addressing critical challenges such as reduced mechanical properties and weaker ITZs in RCA, GO enables the development of high-performance, sustainable concretes. Importantly, the methodology employed in this study using a simple and scalable mixing process enhances the industrial applicability of GO in concrete production while providing scientific base evidence. Further research is recommended to investigate the long-term durability of GO-treated RAC under aggressive environmental conditions and utilising GO for surface treatment of RCA to improve aggregate quality.

CRediT authorship contribution statement

Pasadi Devapura: Writing – review & editing, Writing – original draft, Visualization, Software, Methodology, Investigation, Formal analysis, Data curation. **Thusitha Ginigaddara:** Writing – review & editing, Visualization, Supervision, Methodology, Investigation, Data curation, Conceptualization. **Danula Udumulla:** Writing – review & editing, Visualization, Methodology, Investigation, Data curation. **Priyan Mendis:** Writing – review & editing, Validation, Supervision. **Michael Booy:** Writing – review & editing, Validation. **Nilupa Herath:** Writing – review & editing, Supervision.

Data availability statement

All data generated or used during the study appear in the submitted article.

Declaration of competing interest

The authors declare that they have no known competing financial interests or personal relationships that could have appeared to influence the work reported in this paper.

Acknowledgements

The authors would like to acknowledge Alex Fraser Group for providing materials for this research. Moreover, this work was performed in part at the Materials Characterisation and Fabrication Platform (MCFP) for Nanomaterials characterisation at the University of Melbourne.

Data availability

Data will be made available on request.

References

[1] International Energy Agency, "CO2 Emissions in 2022,", 2022.
[2] Z. Liu, Z. Deng, S. Davis, P. Ciais, Monitoring global carbon emissions in 2022, Nat. Rev. Earth Environ. 4 (4) (2023) 205–206.
[3] International Energy Agency, World Energy Outlook 2019, 2019, pp. 88–95 [Online]. Available: https://www.iea.org/reports/world-energy-outlook-2019.
[4] H. Mountford, et al., COP26: Key Outcomes from the UN Climate Talks in Glasgow, 2021.
[5] A. Akhtar, A.K. Sarmah, Construction and demolition waste generation and properties of recycled aggregate concrete: a global perspective, J. Clean. Prod. 186 (2018/06/10/2018) 262–281, https://doi.org/10.1016/j.jclepro.2018.03.085.
[6] N. Makul, et al., Design strategy for recycled aggregate concrete: a review of status and future perspectives, Crystals 11 (6) (2021) 695 [Online]. Available: https://www.mdpi.com/2073-4352/11/6/695.
[7] C.M. Nwakaire, S.P. Yap, C.C. Onn, C.W. Yuen, H.A. Ibrahim, Utilisation of recycled concrete aggregates for sustainable highway pavement applications; a review, Constr. Build. Mater. 235 (2020) 117444.
[8] S. Han, S. Zhao, D. Lu, D. Wang, Performance improvement of recycled concrete aggregates and their potential applications in infrastructure: a review, Buildings 13 (6) (2023) 1411.
[9] E.O. Fanijo, J.T. Kolawole, A.J. Babafemi, J. Liu, A Comprehensive Review on the Use of Recycled Concrete Aggregate for Pavement Construction: Properties, Performance, and Sustainability, Cleaner Materials, 2023 100199.
[10] Y. Wang, J. Liu, P. Zhu, H. Liu, C. Wu, J. Zhao, Investigation of adhered mortar content on recycled aggregate using image analysis method, J. Mater. Civ. Eng. 33 (9) (2021) 04021225.
[11] K.P. Verian, W. Ashraf, Y. Cao, Properties of recycled concrete aggregate and their influence in new concrete production, Resour. Conserv. Recycl. 133 (2018) 30–49.
[12] A. Abbas, et al., Quantification of the residual mortar content in recycled concrete aggregates by image analysis, Mater. Char. 60 (7) (2009) 716–728.
[13] F. Muhammad, M. Harun, A. Ahmed, N. Kabir, H.R. Khalid, A. Hanif, Influence of bonded mortar on recycled aggregate concrete properties: a review, Constr. Build. Mater. 432 (2024) 136564.
[14] W. Sae-Long, et al., Experimental and simulation analysis of RCA and para-wood ash as partial substitutes for NCA and cement in recycled aggregate concrete, Case Stud. Constr. Mater. 21 (2024) e03716, https://doi.org/10.1016/j.cscm.2024.e03716, 2024/12/01/.
[15] M.J. Chinchillas-Chinchillas, C.A. Rosas-Casarez, S.P. Arredondo-Rea, J.M. Gómez-Soberón, R. Corral-Higuera, SEM image analysis in permeable recycled concretes with silica fume. A quantitative comparison of porosity and the ITZ, Materials 12 (13) (2019) 2201.
[16] Y. Liu, H. Mehdizadeh, T.-C. Ling, Improved concrete ITZ and performance via pre-soaking of inert recycled red brick aggregates in carbonation solution, J. Build. Eng. 86 (2024) 108961.
[17] C. Wang, Z. Du, Microscopic interface deterioration mechanism and damage behavior of high-toughness recycled aggregate concrete based on 4D in-situ CT experiments, Cement Concr. Compos. 153 (2024) 105720.
[18] Y. Liu, P. Ren, N. Garcia-Troncoso, K.H. Mo, T.-C. Ling, Roles of enhanced ITZ in improving the mechanical properties of concrete prepared with different types of recycled aggregates, J. Build. Eng. 60 (2022) 105197.
[19] Q. Huang, et al., Investigation on the properties of aggregate-mastic interfacial transition zones (ITZs) in asphalt mixture containing recycled concrete aggregate, Constr. Build. Mater. 269 (2021) 121257.
[20] H. Wu, C. Liang, Z. Zhang, P. Yao, C. Wang, Z. Ma, Utilizing heat treatment for making low-quality recycled aggregate into enhanced recycled aggregate, recycled cement and their fully recycled concrete, Constr. Build. Mater. 394 (2023) 132126.
[21] S. Ahmad, M. Maslehuddin, M. Shameem, R.M. Faysal, S.K. Adekunle, Effect of abrasion and chemical treatment of recycled aggregate on the workability, strength, and durability properties of concrete, European J. Environ. Civil Eng. 26 (8) (2022) 3276–3291.
[22] M. Yunusa, X. Zhang, P. Cui, X. Tian, Durability of recycled concrete aggregates prepared with mechanochemical and thermal treatment, Materials 15 (16) (2022) 5792.
[23] T. Lv, et al., Review on physical performance, modification mechanisms, carbon emissions and economic costs of recycled aggregates modified with physical enhancement technologies, J. Environ. Manag. 357 (2024/04/01/2024) 120713, https://doi.org/10.1016/j.jenvman.2024.120713.
[24] C. Feng, B. Cui, Y. Huang, H. Guo, W. Zhang, J. Zhu, Enhancement technologies of recycled aggregate–Enhancement mechanism, influencing factors, improvement effects, technical difficulties, life cycle assessment, Constr. Build. Mater. 317 (2022) 126168.
[25] M. Marvila, P. de Matos, E. Rodríguez, S.N. Monteiro, A.R. de Azevedo, Recycled aggregate: a viable solution for sustainable concrete production, Materials 15 (15) (2022) 5276.
[26] T. Ayub, W.M. Asad-ur-Rehman Khan, Effect of recycled concrete aggregates on compressive strength and water permeability of concrete, Int. J. Energy Environ. 14 (2020) 25–32.
[27] F. Fiol, C. Thomas, C. Muñoz, V. Ortega-López, J. Manso, The influence of recycled aggregates from precast elements on the mechanical properties of structural self-compacting concrete, Constr. Build. Mater. 182 (2018) 309–323.
[28] S. Manzi, C. Mazzotti, M.C. Bignozzi, Self-compacting concrete with recycled concrete aggregate: study of the long-term properties, Constr. Build. Mater. 157 (2017) 582–590.
[29] NBR-15116, " Recycled Aggregate of Solid Residue of Building Construtions—Requeriments and Methodologies," Brazilian Association of Technical Standards—ABNT: Rio de Janeiro, Brazil, 2004.
[30] Technical Specification for Application of Recycled Aggregate, JGJ/T-240, 2011.
[31] D.I.N. DIN, "4226-100. Aggregates for concrete and mortar—part 100: recycled aggregates,", Deutsches Institut Fur Normung (2002).
[32] BSI, BS 8500-1: 2015+ A2: 2019. Concrete. Complementary British Standard to BS EN 206. Method of Specifying and Guidance for the Specifier, BSI London, 2019.
[33] Cement Concrete & Aggregates Australia, Use of Recycled Aggregates in Construction, 2008. Australia.
[34] CSIRO, HB 155–2002: Guide to the Use of Recycled Concrete and Masonry Materials, 2002.
[35] L. Li, M. Wu, An overview of utilizing CO2 for accelerated carbonation treatment in the concrete industry, J. CO2 Util. 60 (2022) 102000, https://doi.org/10.1016/j.jcou.2022.102000, 2022/06/01/.
[36] J. Yang, et al., Feasibility of recycled aggregates modified with a compound method involving sodium silicate and silane as permeable concrete aggregates, Constr. Build. Mater. 361 (2022) 129747.

[37] P. Velardo, I.S. del Bosque, M.S. de Rojas, N. De Belie, C. Medina, Durability of concrete bearing polymer-treated mixed recycled aggregate, Constr. Build. Mater. 315 (2022) 125781.
[38] V.W. Tam, H. Wattage, K.N. Le, A. Buteraa, M. Soomro, Methods to improve microstructural properties of recycled concrete aggregate: a critical review, Constr. Build. Mater. 270 (2021) 121490.
[39] F. Farjadian, et al., Recent developments in graphene and graphene oxide: properties, synthesis, and modifications: a review, ChemistrySelect 5 (33) (2020) 10200–10219.
[40] X. Yan, D. Zheng, H. Yang, H. Cui, M. Monasterio, Y. Lo, Study of optimizing graphene oxide dispersion and properties of the resulting cement mortars, Constr. Build. Mater. 257 (2020) 119477.
[41] T. Ginigaddara, P. Mendis, P. Devapura, D. Mohotti, I. Fonseka, Innovative low carbon graphene concrete, Concrete Australia 48 (4) (2022) 33–41.
[42] D. Udumulla, T. Ginigaddara, T. Jayasinghe, P. Mendis, S. Baduge, Effect of graphene oxide nanomaterials on the durability of concrete: a review on mechanisms, provisions, challenges, and future prospects, Materials 17 (10) (2024) 2411.
[43] T. Ginigaddara, J. Ekanayake, P. Mendis, P. Devapura, A. Liyanage, P. Vaz-Serra, An introduction to high performance graphene concrete, Electron. J. Struct. Eng. 22 (3) (2022) 11–18.
[44] Y. Suo, R. Guo, H. Xia, Y. Yang, B. Zhou, Z. Zhao, A review of graphene oxide/cement composites: performance, functionality, mechanisms, and prospects, J. Build. Eng. 53 (2022) 104502.
[45] C. Liu, et al., Advance on the dispersion treatment of graphene oxide and the graphene oxide modified cement-based materials, Nanotechnol. Rev. 10 (1) (2021) 34–49.
[46] L. Zhao, et al., Deep research about the mechanisms of graphene oxide (GO) aggregation in alkaline cement pore solution, Constr. Build. Mater. 247 (2020) 118446.
[47] X. Wang, J. Zhong, Revisiting the strengthening mechanisms of graphene oxide reinforced cement: effects of dispersion states, Cement Concr. Res. 170 (2023) 107189.
[48] G. Jing, et al., The non-uniform spatial dispersion of graphene oxide: a step forward to understand the inconsistent properties of cement composites, Constr. Build. Mater. 264 (2020/12/20/2020) 120729, https://doi.org/10.1016/j.conbuildmat.2020.120729.
[49] Z. Lu, D. Hou, A. Hanif, W. Hao, Z. Li, G. Sun, Comparative evaluation on the dispersion and stability of graphene oxide in water and cement pore solution by incorporating silica fume, Cement Concr. Compos. 94 (2018) 33–42.
[50] S. Ghazizadeh, P. Duffour, N. Skipper, M. Billing, Y. Bai, An investigation into the colloidal stability of graphene oxide nano-layers in alite paste, Cement Concr. Res. 99 (2017) 116–128.
[51] R. Wang, R. Sun, L. Zhao, T. Zhang, X. Kong, Y. Fu, Investigation of the dispersion of reduced graphene oxide in cementitious composites under different mixing strategies, J. Build. Eng. 77 (2023) 107447.
[52] G. Xiong, et al., Effect of power ultrasound assisted mixing on graphene oxide in cement paste: dispersion, microstructure and mechanical properties, J. Build. Eng. 69 (2023) 106321.
[53] S. Chuah, W. Li, S.J. Chen, J.G. Sanjayan, W.H. Duan, Investigation on dispersion of graphene oxide in cement composite using different surfactant treatments, Constr. Build. Mater. 161 (2018) 519–527.
[54] W. Qin, Q. Guodong, Z. Dafu, W. Yue, Z. Haiyu, Influence of the molecular structure of a polycarboxylate superplasticiser on the dispersion of graphene oxide in cement pore solutions and cement-based composites, Constr. Build. Mater. 272 (2021) 121969.
[55] L. Zhao, et al., Investigation of dispersion behavior of GO modified by different water reducing agents in cement pore solution, Carbon 127 (2018/02/01/2018) 255–269, https://doi.org/10.1016/j.carbon.2017.11.016.
[56] C. Liu, et al., Research progress on individual effect of graphene oxide in cement-based materials and its synergistic effect with other nanomaterials, Nanotechnol. Rev. 10 (1) (2021) 1208–1235, https://doi.org/10.1515/ntrev-2021-0080.
[57] B. Liu, L. Wang, G. Pan, D. Li, Dispersion of graphene oxide modified polycarboxylate superplasticizer in cement alkali solution for improving cement composites, J. Build. Eng. 57 (2022) 104860.
[58] W.-J. Long, C. Fang, J. Wei, H. Li, Stability of GO modified by different dispersants in cement paste and its related mechanism, Materials 11 (5) (2018) 834.
[59] A. Anwar, X. Liu, L. Zhang, Enhanced acid resistance of ternary blended concrete composites transformed with graphene oxide for sewer structures, J. Build. Eng. 86 (2024/06/01/2024) 108746, https://doi.org/10.1016/j.jobe.2024.108746.
[60] S.C. Devi, R.A. Khan, Effect of graphene oxide on mechanical and durability performance of concrete, J. Build. Eng. 27 (2020/01/01/2020) 101007, https://doi.org/10.1016/j.jobe.2019.101007.
[61] T. Poinot, K. Benyahia, A. Govin, T. Jeanmaire, P. Grosseau, Use of ultrasonic degradation to study the molecular weight influence of polymeric admixtures for mortars, Constr. Build. Mater. 47 (2013/10/01/2013) 1046–1052, https://doi.org/10.1016/j.conbuildmat.2013.06.007.
[62] L. Silvestro, A.S. Ruviaro, G.T.d.S. Lima, P.R.d. Matos, E. Rodríguez, P.J.P. Gleize, Sonicating polycarboxylate-based superplasticizer for application in cementitious matrix, Revista IBRACON de Estruturas e Materiais 16 (2) (2022) e16205.
[63] L. Djenaoucine, Á. Picazo, M.Á. de la Rubia, A. Moragues, J.C. Gálvez, Influence of graphene oxide on mechanical properties and durability of cement mortar, Materials 17 (6) (2024) 1445.
[64] C. Fang, W. Long, J. Wei, B. Xiao, C. Yan, Effect of graphene oxide on mechanical properties of recycled mortar, in: IOP Conference Series: Materials Science and Engineering, vol. 274, IOP Publishing, 2017 012144, 1.
[65] Y. Xu, Y. Fan, Effect of on graphene oxide the concrete resistance to chloride ion permeability, in: IOP Conference Series: Materials Science and Engineering, vol. 394, IOP Publishing, 2018 032020, 3.
[66] P. Bøggild, Research on scalable graphene faces a reproducibility gap, Nat. Commun. 14 (1) (2023) 1126.
[67] T. Ginigaddara, T. Jayasinghe, P. Mendis, Development of nanomodified graphene concrete using machine learning methods, in: Olympiad in Engineering Science, Springer, 2023, pp. 93–107.
[68] M. Krystek, et al., High-performance graphene-based cementitious composites, Adv. Sci. 6 (9) (2019) 1801195.
[69] N.M. Apandi, W.W.A. Zailani, K.N.K. Izwan, M. Zakaria, N.N. Zulkarnain, Graphene oxide as carbon-based materials: a review of geopolymer with addition of graphene oxide towards sustainable construction materials, Constr. Build. Mater. 411 (2024) 134410.
[70] C. Ruan, J. Lin, S. Chen, K. Sagoe-Crentsil, W. Duan, Effect of graphene oxide on the pore structure of cement paste: implications for performance enhancement, ACS Appl. Nano Mater. 4 (10) (2021) 10623–10633.
[71] W.-J. Long, D. Zheng, H.-b. Duan, N. Han, F. Xing, Performance enhancement and environmental impact of cement composites containing graphene oxide with recycled fine aggregates, J. Clean. Prod. 194 (2018) 193–202.
[72] H. Lv, M. Du, Z. Li, L. Xiao, S. Zhou, Cost optimization of graphene oxide-modified ultra-high-performance concrete based on machine learning methods, Inorganics 12 (7) (2024) 181 [Online]. Available: https://www.mdpi.com/2304-6740/12/7/181.
[73] A. Kedir, M. Gamachu, A.G. Alex, Cement-based graphene oxide composites: a review on their mechanical and microstructure properties, J. Nanomater. 2023 (1) (2023) 6741000.
[74] AS 3972 - 2010 General Purpose and Blended Cements, Standards Australia, Sydney, NSW, Asutralia, 2010.
[75] ASTM C128-22, Standard Test Method for Relative Density (Specific Gravity) and Absorption of Fine Aggregate, American Society Testing and Materials, West Conshohocken, PA, United States, 2022.
[76] ASTM C127-24, Standard Test Method for Relative Density (Specific Gravity) and Absorption of Coarse Aggregate, American Society Testing and Materials, West Conshohocken, PA, United States, 2024.
[77] D. Somaweera, G.A. Abeygunawardane, S. Weragoda, S. Ranatunga, Effect of vein graphite powder on mechanical, curing, and thermal properties of solid tire vulcanizate, Mater. Today Proc. 59 (2022/01/01/2022) 316–323, https://doi.org/10.1016/j.matpr.2021.11.181.
[78] W.S. Hummers Jr., R.E. Offeman, Preparation of graphitic oxide, J. Am. Chem. Soc. 80 (6) (1958), 1339-1339.

[79] H. Zhang, X. Gan, Z. Lu, L. Li, L. Lu, Polycarboxylate superplasticizer-modified graphene oxide: dispersion and performance enhancement in cement paste, Nanomaterials 15 (6) (2025) 419 [Online]. Available: https://www.mdpi.com/2079-4991/15/6/419.
[80] AS 1012, 2:2014 Methods of testing concrete. Preparing Concrete Mixes in the Laboratory, Standards Australia, Sydney, NSW, Asutralia, 2014.
[81] AS 1012.3.1:2014 Methods of testing concrete, Determination of Properties Related to the Consistency of Concrete - Slump Test, Standards Australia, Sydney, NSW, Asutralia, 2014.
[82] AS 1012.9:2014 Methods of testing concrete, Compressive Strength Tests - Concrete, Mortar and Grout Specimens, Standards Australia, Sydney, NSW, Asutralia, 2014.
[83] BS EN 15978, Sustainability of Construction Works - Assessment of Environmental Performance of Buildings - Calculation Method, British Standards Institution, Brussels, 2011.
[84] R. Crawford, A. Stephan, F. Prideaux, Environmental Performance in Construction (EPiC) Database, The University of Melbourne, Melbourne, 2024.
[85] T. Grant, H. Rocha, AusLCI (The Australian Life Cycle Inventory Database Initiative) Database Manual, 2023. Melbourne, no. 1.42.
[86] P. Zandifaez, E. Asadi Shamsabadi, A. Akbar Nezhad, H. Zhou, D. Dias-da-Costa, AI-Assisted optimisation of green concrete mixes incorporating recycled concrete aggregates, Constr. Build. Mater. 391 (2023) 131851, https://doi.org/10.1016/j.conbuildmat.2023.131851, 2023/08/08/.
[87] R. Crawford, A. Stephan, F. Prideaux, EPiC database - gravel, in: Environmental Performance in Construction (EPiC) Database, The University of Melbourne, 2019.
[88] R. Crawford, A. Stephan, F. Prideaux, EPiC database - recycled aggregate, in: Environmental Performance in Construction (EPiC) Database, The University of Melbourne, 2020.
[89] R. Crawford, A. Stephan, F. Prideaux, EPiC database - sand, in: Environmental Performance in Construction (EPiC) Database, The University of Melbourne, 2020.
[90] N.P. Tran, T. Wang, T.N. Nguyen, H. Jin, T.D. Ngo, High-volume recycled glass cementitious and geopolymer composites incorporating graphene oxide, Constr. Build. Mater. 450 (2024/11/08/2024) 138476, https://doi.org/10.1016/j.conbuildmat.2024.138476.
[91] R. Crawford, A. Stephan, F. Prideaux, EPiC database - water, in: Environmental Performance in Construction (EPiC) Database, The University of Melbourne, 2020.
[92] T. Ginigaddara, P. Mendis, P. Devapura, D. Mohotti, I. Fonseka, Innovative low carbon graphene concrete, Concrete Australia 48 (4) (2022) 33–41.
[93] Graphene Labs, Products & services. https://graphenelabs.com.au/. (Accessed 12 March 2025).
[94] P. Zhan, et al., Strength, microstructure and nanomechanical properties of recycled aggregate concrete containing waste glass powder and steel slag powder, J. Clean. Prod. 341 (2022/03/20/2022) 130892, https://doi.org/10.1016/j.jclepro.2022.130892.
[95] P. Zhan, J. Xu, J. Wang, J. Zuo, Z. He, A review of recycled aggregate concrete modified by nanosilica and graphene oxide: materials, performances and mechanism, J. Clean. Prod. 375 (2022) 134116, https://doi.org/10.1016/j.jclepro.2022.134116, 2022/11/15/.
[96] A.S. Alshammari, Controlling dye adsorption kinetics of graphene oxide nano-sheets via optimized oxidation treatment, Crystals 14 (1) (2024) 49 [Online]. Available: https://www.mdpi.com/2073-4352/14/1/49.
[97] Y.-Y. Wu, L. Que, Z. Cui, P. Lambert, Physical properties of concrete containing graphene oxide nanosheets, Materials 12 (10) (2019) 1707.
[98] S. Guo, S. Garaj, A. Bianco, C. Ménard-Moyon, Controlling covalent chemistry on graphene oxide, Nat. Rev. Phys. 4 (4) (2022) 247–262.
[99] G.R. Kumara, et al., Development of a chemical-free floatation technology for the purification of vein graphite and characterization of the products, Sci. Rep. 11 (1) (2021) 22713.
[100] G. Surekha, K.V. Krishnaiah, N. Ravi, R.P. Suvarna, FTIR, Raman and XRD analysis of graphene oxide films prepared by modified Hummers method, in: Journal of Physics: Conference Series, vol. 1495, IOP Publishing, 2020 012012, 1.
[101] Y. Hou, S. Lv, L. Liu, X. Liu, High-quality preparation of graphene oxide via the Hummers' method: understanding the roles of the intercalator, oxidant, and graphite particle size, Ceram. Int. 46 (2) (2020) 2392–2402.
[102] Q.T. Ain, S.H. Haq, A. Alshammari, M.A. Al-Mutlaq, M.N. Anjum, The systemic effect of PEG-nGO-induced oxidative stress in vivo in a rodent model, Beilstein J. Nanotechnol. 10 (1) (2019) 901–911.
[103] D. Dahanayake, et al., Derivatives of Sri Lankan vein graphite: atomic scale study of graphene oxide and reduced graphene oxide, Nanosci. Nanotechnol. - Asia 13 (5) (2023) 41–50.
[104] Q. Zheng, B. Han, X. Cui, X. Yu, J. Ou, Graphene-engineered cementitious composites: small makes a big impact, Nanomater. Nanotechnol. 7 (2017) 1847980417742304.
[105] U.-a. Kanta, V. Thongpool, W. Sangkhun, N. Wongyao, J. Wootthikanokkhan, Preparations, characterizations, and a comparative study on photovoltaic performance of two different types of graphene/TiO2 nanocomposites photoelectrodes, J. Nanomater. 2017 (1) (2017) 2758294.
[106] C.-Y. Huang, et al., Enhancing cementitious composites with functionalized graphene oxide-based materials: surface chemistry and mechanisms, Int. J. Mol. Sci. 24 (13) (2023) 10461.
[107] M. Wang, R. Wang, H. Yao, S. Farhan, S. Zheng, C. Du, Study on the three dimensional mechanism of graphene oxide nanosheets modified cement, Constr. Build. Mater. 126 (2016) 730–739.
[108] D. Hou, T. Yang, J. Tang, S. Li, Reactive force-field molecular dynamics study on graphene oxide reinforced cement composite: functional group de-protonation, interfacial bonding and strengthening mechanism, Phys. Chem. Chem. Phys. 20 (13) (2018) 8773–8789.
[109] D. López-Díaz, M. Lopez Holgado, J.L. García-Fierro, M.M. Velázquez, Evolution of the Raman spectrum with the chemical composition of graphene oxide, J. Phys. Chem. C 121 (37) (2017) 20489–20497.
[110] V. Gupta, N. Sharma, U. Singh, M. Arif, A. Singh, Higher oxidation level in graphene oxide, Optik 143 (2017/08/01/2017) 115–124, https://doi.org/10.1016/j.ijleo.2017.05.100.
[111] E.I. Bîru, H. Iovu, Graphene nanocomposites studied by Raman spectroscopy, Raman Spectrosc 9 (2018) 179.
[112] M.C. Costa, V.S. Marangoni, P.R. Ng, H.T. Nguyen, A. Carvalho, A.H. Castro Neto, Accelerated synthesis of graphene oxide from graphene, Nanomaterials 11 (2) (2021) 551.
[113] J. Park, W. Lee, J. Nam, J.T. Han, C.-J. Choi, J.Y. Hwang, A study of the correlation between the oxidation degree and thickness of graphene oxides, Carbon 189 (2022) 579–585.
[114] A. Salas_Montoya, C.-W. Chung, B.E. Mira_Rada, Interaction effect of recycled aggregate type, moisture state, and mixing process on the properties of high-performance concretes, Case Stud. Constr. Mater. 18 (2023/07/01/2023) e02208, https://doi.org/10.1016/j.cscm.2023.e02208.
[115] H. Zhang, X. Xu, W. Liu, B. Zhao, Q. Wang, Influence of the moisture states of aggregate recycled from waste concrete on the performance of the prepared recycled aggregate concrete (RAC)–A review, Constr. Build. Mater. 326 (2022) 126891.
[116] H. Zhou, D. Li, The dispersion and influence of graphene-oxide-modified polycarboxylate superplasticiser in alkaline cement solution, Adv. Cement Res. (2024) 1–12.
[117] X. Li, et al., Effects of graphene oxide agglomerates on workability, hydration, microstructure and compressive strength of cement paste, Constr. Build. Mater. 145 (2017) 402–410.
[118] V. Ortega-López, V. Revilla-Cuesta, A. Santamaría, A. Orbe, M. Skaf, Microstructure and dimensional stability of slag-based high-workability concrete with steelmaking slag aggregate and fibers, J. Mater. Civ. Eng. 34 (9) (2022) 04022224.
[119] K. Nandanam, U.S. Biswal, P. Dinakar, Effect of fly ash, GGBS, and metakaolin on mechanical and durability properties of self-compacting concrete made with 100% coarse recycled aggregate, J. Hazard. Toxic Radioact. Waste 25 (2) (2021) 04021002.
[120] ASTM C 39/C39M, Standard test method for compressive strength of cylindrical concrete specimens, Am. Soc. Test. Mater. West Conshohocken, PA, United States (2024) 1–7, 2024.
[121] Y.-C. Chang, Y.-Y. Wang, H. Zhang, J. Chen, Y. Geng, Different influence of replacement ratio of recycled aggregate on uniaxial stress-strain relationship for recycled concrete with different concrete strengths, Structures 42 (2022/08/01/2022) 284–308, https://doi.org/10.1016/j.istruc.2022.05.117.

[122] I. Patra, G.R.L. Al-Awsi, Y.M. Hasan, S.S.K. Almotlaq, Mechanical properties of concrete containing recycled aggregate from construction waste, Sustain. Energy Technol. Assessments 53 (2022) 102722.
[123] H. El-Hassan, P. Kianmehr, S. Zouaoui, Properties of pervious concrete incorporating recycled concrete aggregates and slag, Constr. Build. Mater. 212 (2019/07/10/2019) 164–175, https://doi.org/10.1016/j.conbuildmat.2019.03.325.
[124] J. Yang, et al., The influence of graphene oxide on the hydration and mechanical properties of cement-based materials with low water-binder ratio, Cement Concr. Compos. 152 (2024) 105640.
[125] Y. Tu, H. Yu, H. Ma, W. Han, Y. Diao, Experimental study of the relationship between bond strength of aggregates interface and microhardness of ITZ in concrete, Constr. Build. Mater. 352 (2022) 128990, https://doi.org/10.1016/j.conbuildmat.2022.128990, 2022/10/17/.
[126] W. Wang, Y. Liu, L. Jiang, L. Zhao, Z. Li, Effect of physical properties of recycled coarse aggregate on the mechanical properties of recycled aggregate thermal insulation concrete (RATIC), Constr. Build. Mater. 180 (2018/08/20/2018) 229–238, https://doi.org/10.1016/j.conbuildmat.2018.05.232.
[127] L. Yu, S. Bai, X. Guan, Effect of graphene oxide on microstructure and micromechanical property of ultra-high performance concrete, Cement Concr. Compos. 138 (2023) 104964.
[128] J. Góra, M. Szafraniec, Influence of maximum aggregate grain size on the strength properties and modulus of elasticity of concrete, Appl. Sci. 10 (11) (2020) 3918.
[129] R.W. Sun, G.C. Fanourakis, An assessment of factors affecting the elastic modulus of concrete, Struct. Concr. 23 (1) (2022) 593–603.
[130] C. Liang, et al., Enhancing the elastic modulus of concrete prepared with recycled coarse aggregates of different quality by chemical modifications, Constr. Build. Mater. 360 (2022) 129590.
[131] H. Chu, Y. Zhang, F. Wang, T. Feng, L. Wang, D. Wang, Effect of graphene oxide on mechanical properties and durability of ultra-high-performance concrete prepared from recycled sand, Nanomaterials 10 (9) (2020) 1718.
[132] P.V.R.K. Reddy, D.R. Prasad, The role of graphene oxide in the strength and vibration characteristics of standard and high-grade cement concrete, J. Build. Eng. 63 (2023/01/01/2023) 105481, https://doi.org/10.1016/j.jobe.2022.105481.
[133] A.M. Maglad, et al., A study on the properties of geopolymer concrete modified with nano graphene oxide, Buildings 12 (8) (2022) 1066 [Online]. Available: https://www.mdpi.com/2075-5309/12/8/1066.
[134] D.-H. Son, D. Hwangbo, H. Suh, B.-I. Bae, S. Bae, C.-S. Choi, Mechanical properties of mortar and concrete incorporated with concentrated graphene oxide, functionalized carbon nanotube, nano silica hybrid aqueous solution, Case Stud. Constr. Mater. 18 (2023) e01603, https://doi.org/10.1016/j.cscm.2022.e01603, 2023/07/01/.
[135] Y. Zhao, et al., Study of mechanical properties and early-stage deformation properties of graphene-modified cement-based materials, Constr. Build. Mater. 257 (2020) 119498.
[136] H. Guo, R. Gao, S. Liu, C. Feng, M. Qin, G. Sun, Effect of ultra-low dosage graphene oxide on the properties of recycled cement-based materials, J. Build. Eng. 91 (2024) 109637, https://doi.org/10.1016/j.jobe.2024.109637, 2024/08/15/.
[137] S. Kumar, N. Bheel, S. Zardari, A.S. Alraeeini, A.H. Almaliki, O. Benjeddou, Effect of graphene oxide on mechanical, deformation and drying shrinkage properties of concrete reinforced with fly ash as cementitious material by using RSM modelling, Sci. Rep. 14 (1) (2024) 18675.
[138] L. Zhao, X. Guo, L. Song, Y. Song, G. Dai, J. Liu, An intensive review on the role of graphene oxide in cement-based materials, Constr. Build. Mater. 241 (2020) 117939.
[139] K. Guo, J.H. Zhou, M. Liu, L. Liu, Strengthening effect of graphene oxide on mechanical properties of interface transition zone of recycled concrete, Key Eng. Mater. 852 (2020) 49–58.
[140] K. Guo, M. Zhang, Experimental study on fracture energy of graphene oxide recycled concrete, J. Civil Eng. Urban Planning 5 (4) (2023) 41–47.
[141] X. Zifang, D. Tao, G. Chan, Z. Xiang, Y. Dongdong, Study on properties of graphene oxide modified recycled cement-based composites, Integrated Ferroelectrics Int. J. 227 (1) (2022) 132–144.
[142] W. Qidong, Z. Changshun, W. Xudong, A. Zixuan, L. Yeke, Effect of graphene oxide on strength and interfacial transition zone of recycled aggregate concrete, Mater. Res. Express 9 (7) (2022) 075008.
[143] D. Lu, D. Wang, Y. Wang, J. Zhong, Nano-engineering the interfacial transition zone between recycled concrete aggregates and fresh paste with graphene oxide, Constr. Build. Mater. 384 (2023/06/27/2023) 131244, https://doi.org/10.1016/j.conbuildmat.2023.131244.
[144] C. Liu, X. Huang, Y.-Y. Wu, X. Deng, Z. Zheng, The effect of graphene oxide on the mechanical properties, impermeability and corrosion resistance of cement mortar containing mineral admixtures, Constr. Build. Mater. 288 (2021/06/21/2021) 123059, https://doi.org/10.1016/j.conbuildmat.2021.123059.
[145] J.D. Ríos, C. Leiva, A. Martinez de la Concha, M.P. Ariza, H. Cifuentes, Influence of graphene oxide concentration and ultrasonication energy on fracture behavior of nano-reinforced cement pastes, Crystals 14 (8) (2024) 707 [Online]. Available: https://www.mdpi.com/2073-4352/14/8/707.
[146] S. Wu, T. Qureshi, G. Wang, Application of graphene in fiber-reinforced cementitious composites: a review, Energies 14 (15) (2021) 4614.
[147] S. Meng, X. Ouyang, J. Fu, Y. Niu, Y. Ma, The role of graphene/graphene oxide in cement hydration, Nanotechnol. Rev. 10 (1) (2021) 768–778.
[148] H. Zeng, et al., Experiment and modelling of degradation mechanism of cement mortar with graphene oxide nanosheets under sulfate attack, Cement Concr. Compos. 155 (2025) 105833.
[149] F.B. de Souza, X. Yao, W. Gao, W. Duan, Graphene opens pathways to a carbon-neutral cement industry, Sci. Bullet. 67 (1) (2022) 5–8.
[150] T. Schmaltz, L. Wormer, U. Schmoch, H. Döscher, Graphene roadmap briefs (No. 3): meta-market analysis 2023, 2D Mater. 11 (2) (2024) 022002.